Table 2. Genes that show differential expression levels in 44As3 cells as compared with those in HSC-44PE cells

Ratio	Symbol	Gene name	Function and description
Upregulated gene			
29.63	*MMP1*	Matrix metalloproteinase 1	Proteolysis and peptidolysis, collagenase
11.25	*LOC57402*		Cell signaling
9.68	*I_1109564*	H19	Unknown function
4.92	*LGALS1*	Lectin, galactoside-binding, galectin 1	Apoptosis, cell adhesion
4.84	*I_930461*	Tropomyosin 2 (beta)	Contractile proteins
4.47	*AGR2*	Anterior gradient 2 homolog (Xenepus laevis)	Oncogenesis
4.40	*BOK*	BCL2-related ovarian killer	Induction of apoptosis
4.03	*NAP1L4*	Nucleosome assembly protein 1-like 4	Nucleosome assembly
3.99	*TNC*	Tenascin C (hexabrachion)	Binding, cell adhesion
3.98	*HSPB1*	Heat shock 27 kDa protein 1	Regulation of translational initiation
3.95	*HGD*	Homogentisate 1,2-dioxygenase	Tyrosine catabolism, phenylalanine catabolism
3.83	*PIGPC1*		Plasma membrane protein actvated by p53, cell death
3.52	*PIASY*		Apoptosis
3.48	*SYP*	Synaptophysin	Regulating neurotransmitter release
3.38	*RPS12*		Ribosomal protein S12
3.36	*CTSL*	Cathepsin L	Associated with highly invasive tumors
3.35	*HSPC018*		Unknown function
3.23	*INSIG1*	Insulin induced gene 1	Metabolism, cell proliferation
3.20	*I_962761*	Insulin induced gene 1	Metabolism, cell proliferation
3.17	*I_963048*		Immunity
Downregulated gene			
0.14	*THBS1*	Thrombospondin 1	Endopeptidase inhibitor, signal transducer, cell adhesion
0.34	*PRG1*	Proteoglycan 1, secretory granule	Proteoglycan
0.41	*CUL4B*	Cullin 4B	Cell cycle
0.41	*MCM3*	MCM3	Adenosinetriphosphatase, DNA binding
0.42	*NFE2L3*	Nuclear factor (erythroid-derived 2)-like 3	Transcription coactivator, transcription factor
0.43	*THBS4*	Thrombospondin 4	Heparin binding, calcium ion binding, cell adhesion
0.45	*CD59*	CD59 antigen p18–20	Lymphocyte antigen, defense response, signal transduction
0.46	*VBP1*	von Hippel-Lindau binding protein 1	Protein binding
0.46	*LOC51659*		Unkown function
0.47	*PODXL*		Lymphocyte adhesin and homing
0.47	*H2BFB*		H2B histon family member B
0.47	*ZNF195*	Zinc finger protein 195	
0.47	*MCT-1*		Cyclin, cell cycle
0.48	*CD44*	CD44 antigen	Transmembrane glycoprotein, extracellular matrix attachment
0.48	*NDUFA1*	NADH dehydrogenase (ubiquinone)	Energy pathways

kidney also. Although only rarely, pleural effusion and ovarian micrometastases were also noted (data not shown). Orthotopic injection of the parent cell line (HSC-58), however, resulted in the mice becoming moribund approximately 68 days after the implantation (Table 1, Fig. 2E). When the dead animals were autopsied, mild peritoneal dissemination was noted, but ascites were observed in only a very small number of animals (Table 1).

Comparison of gene expression between the highly metastatic- and the parent cell lines. The parent cell lines with a low potential for peritoneal dissemination were compared with the highly metastatic cell lines, using a cDNA microarray (approximately 30 000 genes; Agilent). The differences in the gene expression levels between the two types of cell lines were assessed by measuring the ratios of their expression. The ratio was rated as significant when it was over 2:1. The first 15 genes ranked in terms of this ratio are shown in Tables 2 and 3. When the highly metastatic cell line 44As3 was compared with its parent cell line HSC-44PE, the expression of 89 genes, such as that of MMP1 and cathepsin L, was more intense and that of 19 genes; for example, thrombospondin 1 was less intense in the 44As3 cells in comparison to the parent cell line (Table 2). Table 2 shows the results of a similar comparison of 58As1 and 58As9 cells (highly metastatic cell lines showing a marked increase of proliferative potential) with the parent cell line, HSC-58. Compared to that in the parent cell line, 58As1 cells showed more intense expression of 40 and less intense expression of 20 of the genes examined, while 58As9 cells showed more intense expression of 36 and less intense expression of 32 of the genes examined. In addition to the MMP1 and cathepsin L genes, genes encoding molecules associated with cell adhesion, motility, proliferation, apoptosis, metabolic enzymes and so on, also showed altered expression.

Then, the expression levels of MMP1 and cathepsin L were confirmed at the protein level and compared with the expression levels of known metastasis-associated genes (Table 4). Weak MMP1 protein expression was seen in 44As3 cells as well as 58As9 cells. The cathepsin L gene was expressed in HSC-44PE cells, but even stronger expression was observed in the 44As3 cells (Fig. 3A,B). Intense expression of this gene was also seen in the metastatic cell line, 58As1 (Fig. 3C). Moderate expression of the cathepsin L gene was observed in 58As9 cells, whereas expression of this gene was totally absent in the parent cell line (Fig. 3D). Molecules whose expression levels differed markedly between the parent cell line and the 58As1 or 58As9 cells were dysadherin, CD44, integrin β4, EGFR (Fig. 3E,F), HGF, and VEGF (Fig. 3G,H). While dysadherin was not expressed in the HSC-58 cells, it was expressed intensely in all the highly metastatic subclones (Fig. 3I,J). Intense expression of nm23

Table 3. Genes that show differential expression levels in 58As1 and 58As9 compared with that in HSC-58 cells

Ratio	Symbol	Gene name	Function and description
Upregulated genes 58As1			
19.41	*ADH1C*	Alcohol dehydrogenase 1C, gamma polypeptide	Zinc ion binding, electron transporter, metabolism
18.59	*ADH1B*	Alcohol dehydrogenase IB, beta polypeptide	Zinc ion binding, electron transporter, metabolism
17.70	*FABP1*	Fatty acid binding protein 1, liver	Lipid transporter, fatty acid metabolism, cell signaling
15.21	*ADH1A*	Alcohol dehydrogenase 1A, alpha polypeptide	Zinc ion binding, electron transporter, metabolism
14.15	*PLAT*	Plasminogen activator, tissue	Proteolysis and peptidolysis, blood coagulation
11.01	*MTP*	Microsomal triglyceride transfer protein subunit precursor	Lipid metabolism, Small molecule-binding protein
10.47	*AKR1C2*	Aldo-keto reductase family 1, member C2	Bile acid electron transporter, metabolism
4.71	*CYP1B1*	Cytochrome P450, family 1, subfamily B, polypeptide 1	Cytochrome P450, electron transporter, morphogenesis
4.67	*AKR1C3*	Aldo-keto reductase family 1, member C3	Electron transporter, metabolism, cell proliferation
4.04	*PON2*	Paraoxonase 2	Arylesterase
4.01	*RDHL*		NADP-dependent retinol dehydrogenase/reductase
3.73	*SERPINE2*	Serine proteinase inhibitor, clade E, member 2	Serpin, development
3.60	*PPP1R14A*	Protein phosphatase 1, regulatory subunit 14A	
3.54	*TGFBI*	Transforming growth factor, beta-induced, 68 kDa	Integrin binding, tumor suppressor, cell adhesion
3.45	*PROCR*	Protein C receptor, endothelial (EPCR)	Receptor, inflammatory response
Upregulated genes 58As9			
7.03	*AKR1C2*	Aldo-keto reductase family 1, member C2	Bile acid transporter, binding, electron transporter
6.08	*I_1109564*	H19, imprinted maternally expressed untranslated mRNA	Unknown function
5.95	*MKNK2*	MAP kinase-interacting serine/threonine kinase 2	Phosphorylation, signal transduction
4.10	*APOC1*	Apolipoprotein C-I	Lipid metabolism
4.07	*FLJ21841*		Unknown function
4.02	*SERPINE2*	Serine proteinase inhibitor, clade E, member 2	Serpin, development
3.77	*CTSL*	Cathepsin L	Cathepsin L, associated with highly invasive tumors
3.28	*AKR1C3*	Aldo-keto reductase family 1, member C3	Electron transporter, metabolism, cell proliferation
3.11	*SIAT8B*	Sialyltransferase 8B (alpha-2, 8-sialyltransferase)	Metabolism, embryogenesis and morphogenesis
3.01	*FKBP1B*	FK506 binding protein 1B	Popeptidylprolyl isomerase
2.82	*KIAA1247*		Member of the sulftase family
2.80	*I_1000731*	GRB2-associated binding protein 2	Protein-protein and protein–lipid interactions
2.77	*STMN3*	Stathmin-like 3	Neurogenesis, SCG10 like-protein, tumor progression
2.75	*ANK3*	Ankyrin 3, node of Ranvier (ankyrin G)	Cytoskeletal anchoring, vesicle transport
2.74	*CEBPE*	CCAAT/enhancer binding protein (C/EBP), epsilon	Transcription activating factor, defense response
Downregulation 58As1			
0.11	*LAMR1*	Laminin receptor 1	Signal transduction, cell adhesion, invasive growth
0.13	*S100A4*	S100 calcium binding protein A4	Calcium ion binding, invasive growth
0.15	*RARRES1*	Retinoic acid receptor responder	Negative regulation of cell proliferation
0.15	*HLA-DQB1*	HLA complex, class II, DQ beta 1 precursor	Immune response
0.15	*KLK6*	Kallikrein 6 (neurosin, zyme)	Serine-type peptidase, pathogenesis
0.16	*TM4SF4*	Transmembrane 4 superfamily member 4	Negative regulation of cell proliferation, glycosylation
0.16	*HLA-DRA*	Major histocompatibility complex, class II, DR alpha	Immune response
0.17	*CTNNB1*	Catenin (cadherin-associated pritein), beta 1, 88 kDa	Tumor suppressor, cell adhesion, transcription
0.19	*HLA-DRB3*	Major histocompatibility complex, class II, DR beta 3	Immune response
0.20	*SAT*	Spermidine/spermine N1-acetyltransferase	Diamine N-acetyltransferase, modulates tumorigenicity
0.20	*HLA-DRB5*	Major histocompatibility complex, class II, DR beta 5	Immune response
0.20	*I_966873*		Strong similarity to human HLA-DRB1
0.21	*FOS*	v-fos FBJ murine osteosarcoma viral oncogene homolog	Transcription, methylation, cell growth, oncogenesis
0.21	*I_965396*		Unknown, high similarity to charcterized human AG2
0.22	*CEACAM6*	Carcinoembryonic antigen-related cell adhesion molecule 6	Signal transduction, cell-cell signaling
Downregulation 58As9			
0.06	*CEACAM8*	Carcinoembryonic antigen-related cell adhesion molecule 8	Tumor antigen, immune response, cell adhesion
0.07	*TM4SF3*	Transmembrane 4 superfamily member 3	Signal transducer, tumor antigen, pathogenesis
0.07	*LAMR1*	Laminin receptor 1 (ribosomal protein SA, 67 kDa)	Signal transduction, cell adhesion, invasive growth
0.09	*CEACAM6*	Carcinoembryonic antigen-related cell adhesion molecule 6	Signal transduction, cell-cell signaling, cell adhesion
0.12	*CTNNB1*	Catenin (cadherin-associated pritein), beta 1, 88 kDa	Tumor suppressor, cell adhesion, oncogenesis
0.12	*KRT19*	Keratin 19	Structural constituent of cytoskeleton, differentiation
0.13	*KRTHA3A*	Keratin, hair, acidic, 3 A	Cell shape and cell size control
0.13	*CEACAM3*	Carcinoembryonic antigen-related cell adhesion molecule 3	Tumor antigen, immune response, cell adhesion
0.14	*I_966690*		Strong similarity to human HLA-DRB4
0.17	*S100A4*	S100 calcium binding protein A4	Calcium ion binding, invasive growth
0.20	*FOS*	v-fos FBJ murine osteosarcoma viral oncogene homolog	Transcription, methylation, cell growth, oncogenesis
0.22	*DAF*	Decay accelerating factor for complement (CD55)	Decay accelerating factor
0.23	*MYC*	v-myc myelocytomatosis viral oncogene homolog (avian)	Transcription factor, cell cycle, pathogenesis
0.24	*CRIP1*	Cysteine-rich protein 1 (intestinal)	Zinc ion binding, cell proliferation
0.24	*KRTHB6*	Keratin, hair, basic, 6	Monilethrix

 doi: 10.1111/j.1349-7006.2005.00054.x

Table 4. Expression of metastasis-related genes in the highly metastatic and the parent gastric cancer cell lines

Cell line	MMP-1	Cathepsin L	Cell adhesion					Oncogenes					Angiogenesis				nm23	Smad4
			CD44	E-cadherin	Dysadherin	β-catenin	Integrin α6β4	EGFR	c-erb-B-2	cript	c-met	HGF	bFGF	VEGF	IL-6	IL-8		
44As3	+	++	++a	++	++	++	—	++	–	+	+	–	–	+	–	–	++	–
HSC-44PE	–	+	++a	++	++	++	–++	++	–	+	+	+	–	+	–	–	–	–
58As1	–	++	++	–	++	++	–++	+	–	+	++a	++	+	++	–	–	++	–
58As9	+	+	++	–	++	+	–+	++	–	+	++a	+	+	++	–	–	+	–
HSC-58	–	–	+	–	–	++	—	–	–	+	++a	–	+	–	–	–	–	–

Immunohistochemical staining was carried out as described in a previous study.[8] ++, Moderate or strong staining intensity, or staining of > 75% of the cells; +, weak staining intensity, or staining of < 25% of the cells; –, negative staining, or staining of < 1% of the cells. a, gene amplification.

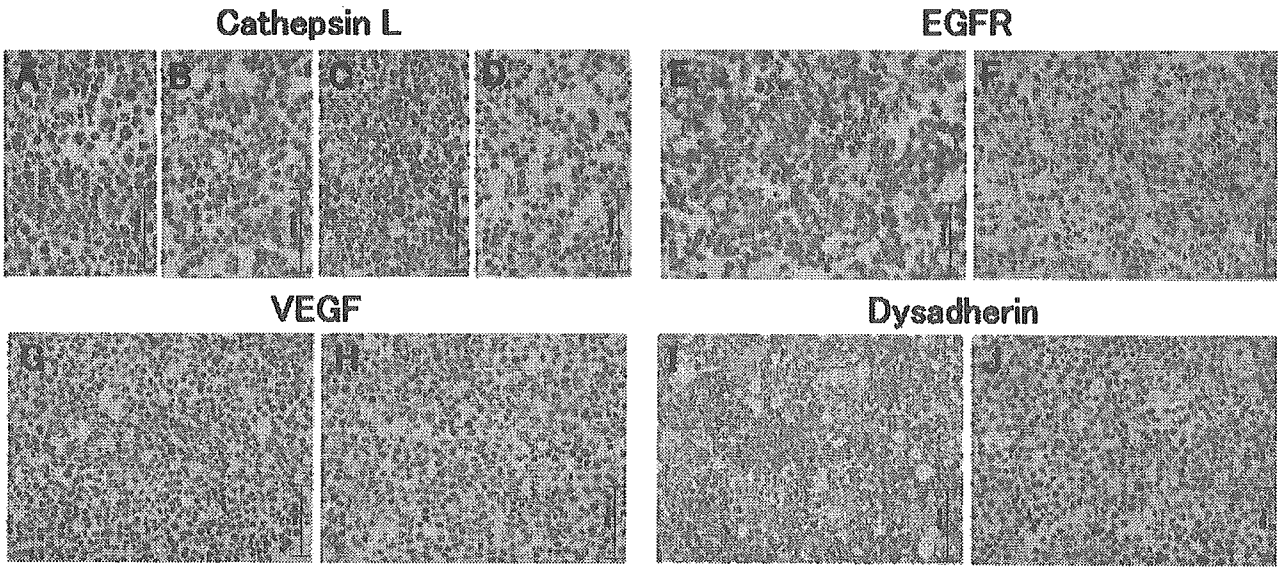

Fig. 3. Immunohistochemical analyses of Cathepsin L, EGFR, VEGF and Dysadherin in the highly metastatic and the parent cell lines. The metastatic 44As3 (A) and 58As1 (C) expressed strongly detectable cathepsin L in the cytoplasm. Immunoreactivity for cathepsin L observed weakly at the cytoplasm in HSC-44PE (B), but immunoreactivity completely absent from HSC-58 (D). (E), Expression of EGER is observed in the membranes of the 58As1 subclone. (F), Immunoreactivity for EGER was completely absent from HSC-58 cells. (G), Expression of VEGF is observed in the cytoplasm of the 58As9 cells, but immunoreactivity absent from HSC-58 (H). (I), Expression of dysadherin is observed at the cell-cell boundaries in 58As9 subclone. (J), Immunoreactivity for dysadherin was completely absent from HSC-58 cells.

was also observed in highly metastatic cell lines, while Smad4 expression was not seen in these cell lines.

Usefulness of the model as a tumor metastasis model for the evaluation of drugs. All of the highly metastatic cell lines served as highly reproducible models of peritoneal dissemination, and a quantitative relationship was observed between the number of inoculated cells and the animal survival rate (incidence of tumor) (data not shown). Next we evaluated antitumor effects of antitumor agents in this model. We selected CPT-11[17] and GEM[18] as representative cytotoxic agents. Figure 4A shows the survival curve of the 58As1 implanted mice treated with CPT-11. Most of the animals belonging to the untreated control group died of extensive peritoneal dissemination approximately 30 days after the implantation. In the CPT-11-treated group (200 mg/kg/head), however, 60 days passed before the first animal death was noted. Thus, treatment with CPT-11 significantly ($P < 0.001$, unpaired t-test) prolonged the survival of the animals injected with the tumor cells, and dose-dependency was evident when the data from multiple groups were compared. Similar results were also obtained for 44As3 cells (Fig. 4B). Figure 4(C) shows the results of the experiment in which GEM was administered intravenously following orthotopic inoculation of 58As1 cells. The survival period was significantly prolonged in the GEM-treated group (100 mg/kg/head). Similar results were also obtained for mice implanted with the 44As3 cells (data not shown).

To identify the stage of tumor metastasis suppressed by these agents, RT-PCR analysis was performed with sets of primers specific for human and mouse β actin, respectively. Cells collected from the intraperitoneal lavage fluid 21 days after orthotopic implantation of 58As1 cells served as the samples. Autopsy examination revealed that there was no macroscopic tumor formation in the gastric wall of the drug-treated animals, while peritoneal dissemination was noted in the untreated control group. Figure 4(D) shows two typical animals used for each experimental group. In the untreated control group, RT-PCR product represents human-derived β actin gene was clearly identified (lanes 3 and 4). In the CPT-11- and GEM-treated groups, however, the gene sequence of human origin was less clear (lanes 5, 6 and 7, 8, respectively). These results suggested that

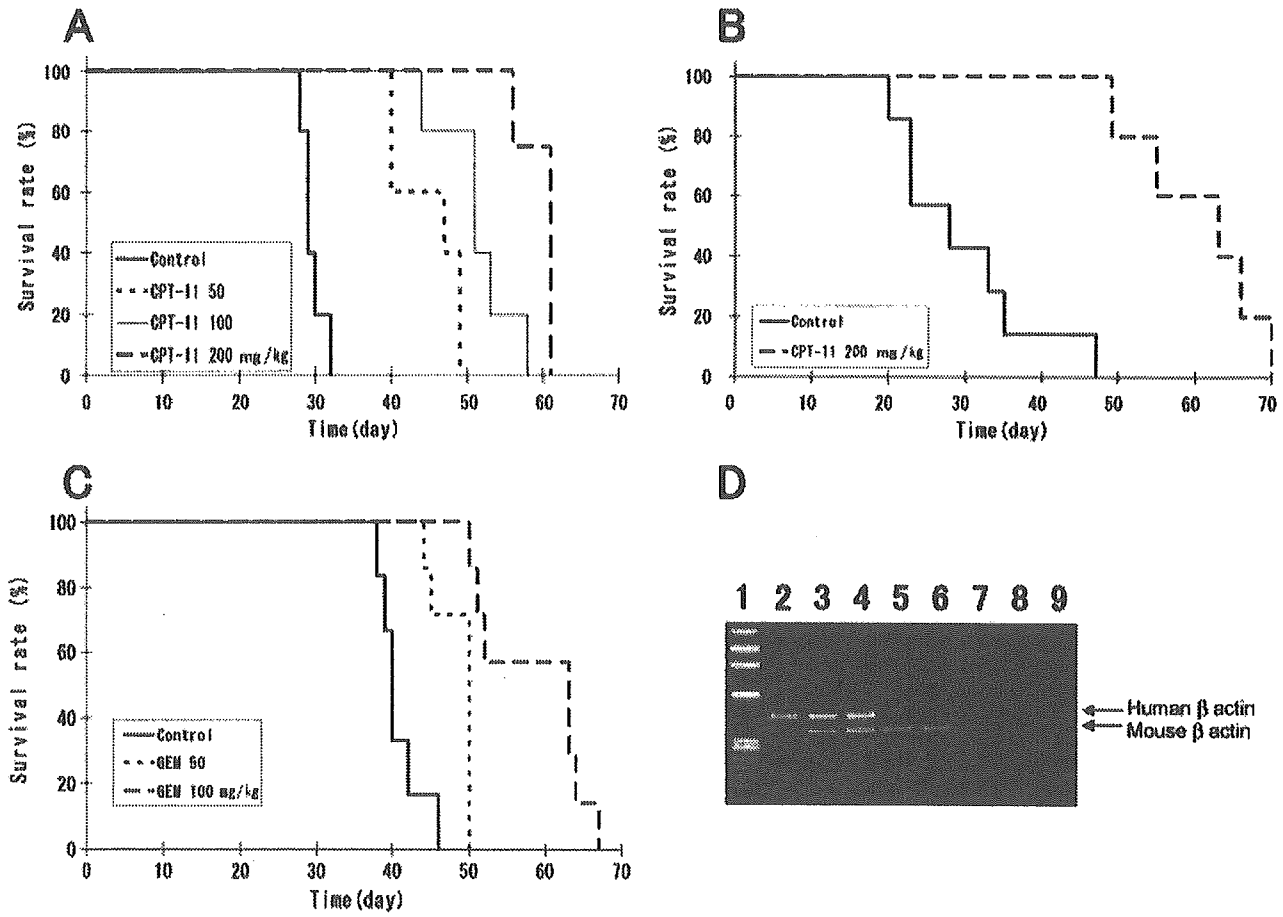

Fig. 4. Effects of CPT-11 and GEM in the peritoneal dissemination mouse model established using orthotopically implanted 44As3 or 58As1 cells. Mice receiving CPT-11 or GEM, or vehicle alone as control, were monitored daily for the development of peritoneal dissemination. (A), Survival of 58As1-tumor-bearing mice after CPT-11 treatment ($n = 5$; $P < 0.001$). This experiment was repeated thrice and similar results were observed each time. (B), Survival of 44As3-tumor-bearing mice after CPT-11 treatment ($n = 6$; $P < 0.001$). (C), Survival of 58As1-tumor-bearing mice after GEM treatment ($n = 7$; $P < 0.001$). Similar results were obtained in two independent experiments. (D), CPT-11 and GEM inhibit dissemination of cancer cells into the peritoneal cavity *in vivo*. RT-PCR was performed on the disseminated cells isolated from the intraperitoneal lavage fluid (2 mL of PBS) using human-specific and mouse-specific primers against β-actin. The total amount of RNA (200 ng) was equalized in all the samples. Lane 1, maker; lane 2, human gastric cell line HSC-39; lanes 3 and 4, untreated control group; lanes 5 and 6, 200 mg/kg CPT-11-treated group; lanes 7 and 8, 100 mg/kg GEM-treated group; lane 9, murine leukemia cell line P388.

treatment with the agents reduced the number of cancer cells in the peritoneal cavity. It was also found that the drugs directly inhibited the growth of s.c. tumors following implantation of 58As1 and 44As3 cells (data not shown). From these results, it is considered highly likely that while the agents suppress metastasis of these tumor cells by suppressing tumor formation at the implanted site, the small number of tumor cells remaining within the peritoneal cavity gradually proliferate, making it difficult to obtain better therapeutic results than some prolongation of the survival period.

Discussion

In the present study, we isolated 44As3 cells from HSC-44PE, and 58As1 and 58As9 cells from HSC-58, and succeeded, in a reliable manner, in establishing a model in which peritoneal dissemination occurred from a primary lesion of gastric carcinoma. The 44As3, 58As1 and 58As9 sublines were generated by the conventional method, that is by selection of highly metastatic clones (found in small numbers among cancer cells showing poor metastatic potential) *in vivo*.[19] On the basis of a study using clinical samples for microarray analysis of primary and metastatic lesions, investigators recently suggested that primary cancers with a high metastatic potential may differ in nature from those having a poor metastatic potential.[20] However, the results of our study support the conventional view that clones with a high metastatic potential contained in small amounts among the cancer tissues are responsible for the formation of metastatic lesions.

We consider that the establishment of this model is significant in the following respects: (i) it allows reproduction of all the steps in the development of cancerous peritonitis, from the stage of infiltrative growth of the tumor within the gastric mucosa to peritoneal dissemination and formation of ascites; (ii) it is an animal model of metastatic gastric cancer that closely resembles that in clinical cases; (iii) quantitative analysis is possible with this model, because it is established from cultured cells. The model is expected to be useful for the study of the continuity or association between infiltrative growth/peritoneal dissemination and gene expression, mechanism of formation of bloody ascites, and analysis of the microenvironmental factors influencing the development of the metastases. Comparison of the expression

 doi: 10.1111/j.1349-7006.2005.00054.x

levels of the relevant genes among different cell lines with markedly varying metastatic potential may be expected to allow isolation of new molecules involved in the peritoneal dissemination of tumors. Furthermore, these sublines are also expected to contribute to advancement of the functional analysis of the involvement of the newly identified molecules in peritoneal dissemination.

Following recent advances in the comprehensive analysis of gene expression, it has been gradually revealed that gene expression patterns undergo complex alterations during the course of metastasis of gastric carcinoma.[21–27] cDNA array analysis carried out using cell lines with varying metastatic potentials in the present study revealed altered expressions of numerous genes in these cells, including those involved in adhesion, proliferation and metabolism. Among others, markedly increased expression of the MMP1 gene[27,28] was observed in 44As3 cells; however, the expression of MMP1 at the protein level was low in these cells, suggesting that MMP1 may not be closely involved in metastasis. Cathepsin L, involved in the degradation of the extracellular matrix,[29] was intensely expressed in not only 44As3, but also 58As1 cells. This finding was confirmed by immunostaining. Intense cathepsin L expression was also seen in 58As9 cells. These results suggest that this molecule may be closely associated with the metastatic potential of these tumor cells. Meanwhile, it is known that invasion and metastasis of gastric cancer occur as a result of accumulation of changes in several genes.[21] These include genes encoding cell adhesion-related molecules (E-cadherin,[30,31] β-catenin,[30] integrin α6β4,[8] dysadherin,[32] CD44,[33,34] etc.), molecules associated with proliferation, loss of intercellular adhesion and matrix degradation (EGF, c-erbB-2,[35] cript,[36] etc.), motility-associated molecules (HGF, c-met,[37] etc.), molecules associated with vascularization (VEGF,[38] IL-6,[39] IL-8,[40] bFGF,[41] etc.), a tumor metastasis suppressor gene (nm23)[42] a gene associated with the malignant course of tumors (Smad),[43] and so on. When the expression of these genes was analyzed, markedly increased expression of MMP1, cathepsin L and nm23 was observed in the highly metastatic 44As3 cell line as compared with that in the poorly metastatic parent cell line. Molecules expressed specifically in the highly metastatic cell lines 58As1 and 58As9 included cathepsin L, dysadherin, CD44, integrin β4, EGFR, HGF and VEGF. Although these molecules seemed to be closely related to peritoneal dissemination of gastric carcinoma, it would be desirable to determine the exact causal relationship between these molecules and tumor metastasis using *in vivo* models. Nonetheless, our results suggest that: (i) there may be multiple pathways involving different molecules for the apparently single process of tumor metastasis, and (ii) the genes contributing to the metastatic potential of tumor cells may differ between the parent cells and the clones selectively isolated from it.

As stated, the presence of peritoneal metastasis represents an advanced stage of cancer associated with a poor prognosis, and no effective therapy for this condition is available as yet. It is therefore important to devise a new therapeutic strategy based on the aforementioned novel viewpoints. One such strategy that has been discussed is the development of anticancer agents based on molecular targeting. To seek such agents, a model allowing appropriate evaluation of drugs is essential, and models to be used for drug evaluation *in vivo* need to satisfy the following six requirements: (i) the tumor should undergo proliferation, spread, dissemination and metastasis akin to those seen in clinical cases; (ii) the tumor cell survival rate in the gastric wall following orthotopic implantation should be 100%; (iii) the frequency of metastasis should be 90–100%; (iv) the model should be highly reproducible; (v) the interindividual variance should be small, to allow easy comparison among different test groups; (vi) application to experiments using many animals should be relatively easy. When the animal model of peritoneal dissemination established in this study was evaluated according to these criteria, all the three highly metastatic cell lines established satisfied all of these six requirements. We evaluated the antitumor activities of two antitumor agents (CPT-11[17] and GEM[18]) using the animal models implanted with 58As1 and 44As3 cells. Treatment with these agents suppressed the proliferation and spread of the tumor and significantly prolonged the survival of the animals. For each of the cases studied, a dose-response relationship was observed, and the experiments were highly reproducible. Another advantage of this animal model is that the length of time from implantation to tumor formation is short (causing death within 40 days); this feature may be expected to contribute to shortening of the evaluation period. The advantages of this model may prove to be useful for the development of drugs based on molecular targeting.

In the past, no approach was known for isolation of host factors involved in the cascade of tumor proliferation in the primary lesion to formation of ascites, or for the functional analysis of this cascade (e.g. analysis of interactions). The model established in the present study is expected to contribute greatly to the advancement of studies in these fields and in other applied research.

Acknowledgments

We are grateful to Dr A. Ochiai (Pathology Division, National Cancer Center Research Institute East) for fruitful discussions. This study was supported in part by a Grant-in-Aid for Cancer Research from the Ministry of Health, Labor and Welfare of Japan.

References

1 Japanese Gastric Cancer Association. Japanese Classification of Gastric Carcinoma – 2nd English Edition. *Gastric Cancer* 1998; **1**: 10–24.
2 Tahara E. Endocrine tumors of the gastrointestinal tract: classification, function and biological behavior. In: Watanabe S, Wolff M, Sommers SC, eds. *Digestive Disease Pathology*. Philadelphia: Field andWood, 1988; 121–47.
3 Fenoglio-preier C, Carneiro F, Correa P *et al.* Gastric carcinoma. In: Hamilton SR, Aaltonen LA, eds. *World Health Organization Classification of Tumours. Pathology and Genetics of Tumours of the Digestive System*. Lyon: IARC Press, 2000; 37–52.
4 Maruyama K. Results of surgery correlated with staging. In: Preece PE, Cuschieri A, Wellwood JM, eds. *Cancer of the Stomach*. Orlando: Grune and Stratton, 1986; 145–63.
5 Moriguchi S, Maehara Y, Korenaga D, Sugimachi K, Nose Y. Risk factors which predict pattern of recurrence after curative surgery for patients with advanced gastric cancer. *Surg Oncol* 1992; **1**: 341–6.
6 Yashiro M, Chung YS, Nishimura S, Inoue T, Sowa M. Peritoneal metastatic model for human scirrhous gastric carcinoma in nude mice. *Clin Exp Metastasis* 1996; **14**: 43–54.
7 Fujita S, Suzuki H, Kinoshita M, Hirohashi S. Inhibition of cell attachment, invasion and metastasis of human carcinoma cells by anti-integrin β1 subunit antibody. *Jpn J Cancer Res* 1992; **83**: 1317–26.
8 Ishii Y, Ochiai A, Yamada T *et al.* Integrin α6β4 as a suppressor and a predictive marker for peritoneal dissemination in human gastric cancer. *Gastroenterology* 2000; **118**: 497–506.
9 Kotanagi H, Saito Y, Shinozawa N, Koyama K. Establishment of a human cancer cell line with high potential for peritoneal dissemination. *J Gastroenterol* 1995; **30**: 437–8.
10 Kaneko K, Yano M, Tsujinaka T *et al.* Establishment of a visible peritoneal micrometastatic model from a gastric adenocarcinoma cell line by green fluorescent protein. *Int J Oncol* 2000; **16**: 893–8.
11 Yanagihara K, Seyama T, Tsumuraya M, Kamada N, Yokoro K. Establishment and characterization of human signet ring cell gastric carcinoma cell lines with amplification of the c-myc oncogene. *Cancer Res* 1991; **51**: 381–6.
12 Yanagihara K, Kamada N, Tsumuraya M, Amano F. Establishment and characterization of a human gastric scirrhous carcinoma cell line in serum-free chemically defined medium. *Int J Cancer* 1993; **54**: 200–7.
13 Yanagihara K, Ito A, Toge T, Numoto M. Antiproliferative effects of

isoflavones on human cancer cell lines established from the gastrointestinal tract. *Cancer Res* 1993; **53**: 5815–21.
14 Yanagihara K, Tanaka H, Takigahira M *et al.* Establishment of two cell lines from human gastric scirrhous carcinoma that possess the potential to metastasize spontaneously in nude mice. *Cancer Sci* 2004; **95**: 575–82.
15 Luo L, Salunga RC, Guo H *et al.* Gene expression profiles of laser-captured adjacent neuronal subtypes. *Nat Med* 1999; **5**: 117–22.
16 Hughes TR, Mao M, Jones AR *et al.* Expression profiling using microarrays fabricated by an ink-jet oligonucleotide synthesizer. *Nat Biotechnol* 2001; **19**: 342–7.
17 Kanzawa F, Saijo N. *In vitro* interaction between gemcitabine and other anticancer drugs using a novel three-dimensional model. *Semin Oncol* 1997; **24**: S7–8–S7–16.
18 Saijo N. Preclinical and clinical trials of topoisomerase inhibitors. *Ann N Y Acad Sci* 2000; **922**: 92–9.
19 Fidler IJ. Rationale and methods for the use of nude mice to study the biology and therapy of human cancer metastasis. *Cancer Metast Rev* 1986; **5**: 29–49.
20 Ramaswamy S, Ross KN, Lander ES, Golub TR. A molecular signature of metastasis in primary solid tumors. *Nat Genet* 2003; **33**: 49–54.
21 Yokozaki H, Yasui W, Tahara E. Genetic and epigenetic changes in stomach cancer. *Int Rev Cytol* 2001; **204**: 49–95.
22 Yasui W, Oue N, Ito R, Kuraoka K, Nakayama H. Search for new biomarkers of gastric cancer through serial analysis of gene expression and its clinical implications. *Cancer Sci* 2004; **95**: 385–92.
23 Hippo Y, Yashiro M, Ishii M *et al.* Differential gene expression profiles of scirrhous gastric cancer cells with high metastatic potential to peritoneum or lymph nodes. *Cancer Res* 2001; **61**: 889–95.
24 Hippo Y, Taniguchi H, Tsutsumi S *et al.* Global gene expression analysis of gastric cancer by oligonucleotide microarrays. *Cancer Res* 2002; **62**: 233–40.
25 Hasegawa S, Furukawa Y, Li M *et al.* Genome-wide analysis of gene expression in intestinal-type gastric cancers using a complementary DNA microarray representing 23 040 genes. *Cancer Res* 2002; **62**: 7012–7.
26 Weiss MM, Kuipers EJ, Postma C *et al.* Genomic profiling of gastric cancer predicts lymph node status and survival. *Oncogene* 2003; **22**: 1872–9.
27 Inoue T, Yashiro M, Nishimura S *et al.* Matrix metalloproteinase-1 expression is a prognostic factor for patients with advanced gastric cancer. *Int J Mol Med* 1999; **4**: 73–7.
28 Sakurai Y, Otani Y, Kameyama K *et al.* Therole of stromal cells in the expression of interstitial collagenase (matrix metalloproteinase-1) in the invasion of gastric cancer. *J Surg Oncol* 1997; **66**: 168–72.
29 Dohchin A, Suzuki JI, Seki H, Masutani M, Shiroto H, Kawakami Y. Immunostained cathepsins B and L correlate with depth of invasion and different metastatic pathways in early stage gastric carcinoma. *Cancer* 2000; **89**: 482–7.
30 Hirohashi S. Inactivation of the E-cadherin-mediated cell adhesion system in human cancers. *Am J Pathol* 1998; **153**: 333–9.
31 Behrens J, Mareel MM, Van Roy FM, Birchmeier W. Dissecting tumor cell invasion: epithelial cells acquire invasive: properties after the loss of uvomorulin-mediated cell-cell adhesion. *J Cell Biol* 1989; **108**: 2435–47.
32 Ino Y, Gotoh M, Sakamoto M, Tsukagoshi K, Hirohashi S. Dysadherin, a cancer-associated cell membrane glycoprotein, down-regulated E-cadherin and promotes metastasis. *Proc Natl Acad Sci USA* 2002; **99**: 365–70.
33 Yokozaki H, Ito R, Nakayama H, Kuniyasu H, Taniyama K, Tahara E. Expression of CD44 abnormal transcripts in human gastric carcinomas. *Cancer Lett* 1994; **83**: 229–34.
34 Nishimura S, Chung YS, Yashiro M, Inoue T, Sowa M. CD44H plays an important role in peritoneal dissemination of scirrhous gastric cancer cells. *Jpn J Cancer Res* 1996; **87**: 1235–44.
35 Tsugawa K, Yonemura Y, Hirono Y *et al.* Amplification of the c-met, c-erbB-2 and epidermal growth factor receptor gene in human gastric cancers: correlation to clinical features. *Oncology* 1998; **55**: 475–81.
36 Kunuyasu H, Yoshida K, Yokozaki H *et al.* Expression of cript, a novel gene of the epidermal growth factor family, in human gastrointestinal carcinomas. *Jpn J Cancer Res* 1991; **82**: 969–73.
37 Kunuyasu H, Yasui W, Yokozaki H, Kitadai Y, Tahara E. Aberrant expression of c-met mRNA in human gastric carcinomas. *Int J Cancer* 1993; **55**: 72–5.
38 Takahashi Y, Cleary KR, Mai M, Kitadai Y, Bucana CD, Ellis LM. Significance of vessel count and vascular endothelial growth factor and its receptor (KDR) in intestinal-type gastric cancer. *Clin Cancer Res* 1986; **2**: 1679–84.
39 Huang SP, Wu MS, Wang HP, Yang PS, Kuo ML, Lin JT. Correlation between serum levels of interleukin-6 and vascular endothelial growth factor in gastric carcinoma. *J Gastroenterol Hepatol* 2002; **17**: 1165–9.
40 Kitadai Y, Haruma K, Sumii K *et al.* Regulation of angiogenesis in human gastric carcinomas by interleukin-8. *Am J Pathol* 1998; **152**: 93–100.
41 Ueki T, Koji T, Tamiya S, Nakane PK, Tsuneyoshi M. Expression of basic fibroblast growth factor and fibroblast growth factor in advanced gastric carcinoma. *J Pathol* 1995; **177**: 353–61.
42 Nakayama H, Yasui W, Yokozaki H, Tahara E. Reduced expression of nm23 is associated with metastasis of human gastric carcinomas. *Jpn J Cancer Res* 1993; **84**: 184–90.
43 Ijichi H, Ikenoue T, Kato N *et al.* Systemic analysis of the TGF-beta-smad signaling pathway in gastrointestinal cancer cells. *Biochem Biophys Res Commun* 2001; **289**: 350–7.

 doi: 10.1111/j.1349-7006.2005.00054.x

Physiol Genomics 22: 8–13, 2005.
First published March 29, 2005; 10.1152/physiolgenomics.00142.2004.

Gene expression profiling of cerebellar development with high-throughput functional analysis

Sakae Saito,[1] Kimi Honma,[2] Hiroko Kita-Matsuo,[1] Takahiro Ochiya,[3] and Kikuya Kato[4]

[1]*Taisho Laboratory of Functional Genomics, Nara Institute of Science and Technology, and Core Research for Evolutional Science and Technology, Japan Science and Technology Corporation;*
[2]*Koken Bioscience Institute, Tokyo;* [3]*National Cancer Center Research Institute, Tokyo; and*
[4]*Research Institute, Osaka Medical Center for Cancer and Cardiovascular Diseases, Osaka, Japan*

Submitted 15 June 2004; accepted in final form 24 March 2005

Saito, Sakae, Kimi Honma, Hiroko Kita-Matsuo, Takahiro Ochiya, and Kikuya Kato. Gene expression profiling of cerebellar development with high-throughput functional analysis. *Physiol Genomics* 22: 8–13, 2005. First published March 29, 2005; 10.1152/physiolgenomics.00142.2004.—We measured the expression levels of 450 genes during mouse postnatal cerebellar development by quantitative PCR using RNA purified from layers of the cerebellar cortex. Principal component analysis of the data matrix demonstrated that the first and second components corresponded to general levels of gene expression and gene expression patterns, respectively. We introduced 288 of the 450 genes into PC12 cells using a high-throughput transfection assay based on atelocollagen and determined the ability of each gene to promote neurite outgrowth or cell proliferation. Five genes induced neurite outgrowth, and seven genes enhanced proliferation. Evaluation of the functional data and gene expression patterns showed that none of these genes exhibited elevated expression at maturation, suggesting that genes characteristic of mature neurons are not likely to participate in neuronal development. These results demonstrate that functional data can facilitate interpretation of expression profiles and identification of new molecules that participate in biological processes.

adaptor-tagged competitive polymerase chain reaction; cell transfection array

DEVELOPMENTAL PROCESSES are executed by intrinsic programs encoded in the genome with modulation by extrinsic factors. Because the execution of such programs is, for the most part, dependent on gene expression, it should be possible to directly elucidate the programs by analyzing gene expression. Conventional approaches such as genetic studies based on mutant analysis have so far identified genes responsible for particular developmental processes. Many of these genes are transcription factors such as homeotic genes; however, many of the molecular events downstream of the transcription factors still remain to be elucidated.

Although gene expression profiling is expected to shed light upon downstream molecular events, the lack of valid information regarding gene functions makes it difficult to interpret the expression data. Complementary methods of analysis include bioinformatics of the scientific literature (24) and proteomics (7, 10). However, direct analysis of gene function is more desirable. Recently, two techniques for high-throughput cell transfection have been described: reverse transfection (33) and a cell transfection array using atelocollagen (16). These two techniques enable large-scale experiments to study the overexpression or suppression of genes.

In this report, we measured the expression levels of 450 cerebellar genes using RNA purified from each layer of the cerebellar cortex. In parallel, we analyzed 288 of the 450 genes by cell transfection array using PC12 cells. The cerebellar cortex is a classic model system in developmental biology (2). The postnatal development of the cerebellum includes most of the events characteristic of nervous system development including axon elongation, cell proliferation, cell migration, synapse formation, and apoptosis. PC12 cells are also a classic model system of neuronal differentiation (13). This cell line is derived from the rat pheochromocytoma, and the cells extend neurites under appropriate stimulation, such as treatment with nerve growth factor (NGF). Combined use of these classical systems has allowed the description of both the transcriptional and functional aspects of nervous system development, demonstrating the correlation between gene expression and function.

MATERIALS AND METHODS

Genes subjected to analysis. We have previously performed gene expression profiling of postnatal cerebellar development using the whole cerebellum (22). This experiment analyzed 1,869 genes selected by descending order of abundance from our expressed sequence tag collection (21). Of these 1,869 genes, 768 genes, including 384 genes whose expression changed during development and 384 genes that were previously reported to be involved in brain development, were selected for the present study (22). Because RNA quantitation using samples recovered by laser capture microdissection (LCM) is demanding, we succeeded in analyzing only 450 of the 768 genes. The full-length cDNAs of 288 of these genes were subcloned into expression vectors. It should be noted that the selected genes may be biased toward abundance but should not be biased to other factors such as gene function or annotation.

LCM. With the use of a PixCell LCM microscope (Arcturus Engineering), the granule cell layers corresponding to the distinct areas described in the main text were dissected from hematoxylin-eosin-stained 12-μm frozen tissue sections of 4-, 8-, 12-, and 21-day-old mice. Three mice were used for LCM at each age. Experimental details are described in protocols for microdissection and RNA preparation on the NIH LCM web page (http://dir.nichd.nih.gov/lcm/lcm.htm). Approximately 100 ng of total RNA were obtained from 1,000 transfer shots of the external granular layer (EGL) and the internal granular layer (IGL).

Adaptor-tagged competitive PCR and data analysis. The adaptor-tagged competitive PCR (ATAC-PCR) protocol is essentially the same as described previously (18, 22, 30). Total RNA from the

Article published online before print. See web site for date of publication (http://physiolgenomics.physiology.org).

Address for reprint requests and other correspondence: K. Kato, Research Institute, Osaka Medical Center for Cancer and Cardiovascular Diseases, 1-3-2 Nakamichi, Higashinari-ku, Osaka 537-8511, Japan (E-mail: katou-ki@mc.pref.osaka.jp).

cerebrum at postnatal *week 6* was used as a standard. The relative expression levels versus the 6-wk cerebrum were calculated. Among the 768 genes subjected to ATAC-PCR, 450 genes had no missing values. This data matrix was normalized as previously described (25). In brief, the data were first divided by the median of the samples and converted into a logarithmic scale. The cutoff values were set at 20 and 0.05 before the logarithmic conversion. Principal component analysis (PCA) was performed using GeneMath 2.0 (AppliedMath).

The chance of biased distribution of functional genes (P) was calculated using the hypergeometric distribution, described as follows:

$$P = 1 - \sum_{x=0}^{m-1} \frac{({}_M\mathrm{C}_x) \times ({}_{N-M}\mathrm{C}_{n-x})}{{}_N\mathrm{C}_n}$$

where N is the number of genes in the total population, M is the number of functional genes in the total population, n is the number of genes in a particular group, and m is the number of functional genes in the group.

Culture and differentiation of PC12 cells. PC12 cells, obtained from the American Type Culture Collection, were grown in DMEM with 10% charcoal-stripped horse serum (Biofluid), 5% dialyzed FBS (GIBCO-BRL), 10 mM HEPES (pH 7.4), 50 mg/ml streptomycin, and 50 U/ml penicillin. To differentiate PC12 cells, 1×10^5 cells were seeded on poly-L-orinithine (Sigma)-coated 25-cm^2 culture flasks. The following day, cells were incubated in PC12 medium containing 100 ng/ml of 2.5S NGF (Collaborative Biomedical Products) for 1 wk. Medium was replaced every 3 days. On *day 7*, neurite extension was clearly observed in >90% cells. *Passage 24* clones were used in all the experiments.

Atelocollagen complex and gene transfer. The full-length open reading frames of 288 genes were amplified from 8-day-old mouse cerebellar cDNA. Because the 8-day-old mouse cerebellum contains both the EGL and the IGL, the selected genes were well amplified and subcloned into pDEST26 using Gateway Technology (Invitrogen). Each purified pDEST26x plasmid and a pCMV-EGFP plasmid were mixed with Atelocollagen (Koken) and dissolved in PBS(−) buffer at a fixed concentration of 80 μg/ml. Each plasmid DNA was used at a concentration of 5 μg/ml. The mixture was incubated for 20 min at 4°C. A small aliquot of the mixture, up to 50 μl, was spotted into a flat-bottom 96-well plate and precoated. PC12 cells were precultured and seeded at 2×10^4 cells/well for transfection of pDESTx and pCMV-EGFP. Green fluorescent protein (GFP) gene expression was monitored by fluorescence microscopy. The transfection efficiency calculated by counting the GFP-positive cells was 29.3 ± 4.51%. Neurite outgrowth was investigated using the Neurite Outgrowth HitKit assay (Cellomics). The signal intensity of the fluorescent stain was detected by the ArrayScan II system (Cellomics) and analyzed using Neurite Outgrowth Application software (Cellomics) under the default parameter setting. The results of the computer analysis were confirmed by microscopic observation. Cellular proliferation was investigated using the TetraColor One cell proliferation assay reagent (Seikagaku) according to the recommended protocol. The colorimetric reaction was assessed by measuring the absorption of each well at 450 nm with a reference wavelength at 650 nm and a ultraviolet microplate reader (Bio-Rad Laboratories). Most of the genes exhibited absorbances around 0.4 (absorbance 450/630 nm). Absorption values of the genes exhibiting growth promotion properties exceeded 0.7.

RESULTS

Gene expression profiling using RNA purified from granule cell layers. In rodents, the development of the cerebellar cortex begins just after birth; the peak of granule cell proliferation occurs during the first week, and the peak of cell migration and axon elongation occurs during the second week (2). The developing granule cell layer typically consists of two sublayers: the EGL and the IGL. Furthermore, the EGL and IGL typically consist of two areas. The proliferating granule cells are located in the superficial area of the EGL (represented as EGLa in Fig. 1), whereas postmitotic and migrating granule cells are located in the internal area of the EGL (EGLb). These granule cells migrate to the IGL, extending parallel fibers. The synaptogenic granule cells are located in the IGL adjacent to the Purkinje cell layer (IGLa), and the mature granule cells are located in the internal area of the IGL (IGLb). The morphological changes in these cells are complete by the third week (2) and regarded as the mature cerebellum. The 21-day cerebellum therefore only consists of IGLb and has the structure as the same as that of an adult. Using LCM, we dissected the granule cell layers from 4-, 8-, 12-, and 21-day-old mice, collecting a total of 12 samples (4-day EGLa, 4-day EGLb, 4-day IGL, 8-day EGLa, 8-day EGLb, 8-day IGLa, 8-day IGLb, 12-day EGL, 12-day IGLa, 12-day IGLb, 21-day IGLa, and 21-day IGLb). It should be noted that we were not able to discriminate among the four layers in some samples because the fraction of EGL decreases and the fraction of IGL increases as development proceeds. The relative expression levels of the 450 genes were obtained using ATAC-PCR. ATAC-PCR is an advanced version of quantitative PCR and has been established as a mature expression profiling technique in several studies (30). The data matrix consisting of 450 genes × 12 samples is supplied as supplementary data (http://physiolgenomics.physiology.org/cgi/content/full/00142.2004/DC1).

We applied several unsupervised feature extraction methods to the data matrix. PCA, a statistical technique to summarize a multivariate data set using a few components, was successful. This analysis demonstrated that the first and second components corresponded to general levels of gene expression and to gene expression patterns, respectively (Fig. 1, *A* and *B*). Sorting of genes by the factor scores of the second component ordered the genes from those elevated during development to those elevated at maturation. In contrast to the prominent temporal changes, differences between the layers were obscure.

Cell transfection array. Postnatal cerebellar development includes cell proliferation and axon elongation. Genes involved in these processes are expected to induce phenotypic changes in PC12 cells; 288 of the 450 cerebellar genes that were subjected to gene expression analysis were also transfected into PC12 cells. To enable high-throughput functional analysis, we employed a cell transfection array using atelocollagen. Atelocollagen is a biocompatible natural polymer that is free of telopeptides and is obtained by pepsin treatment of highly purified type I collagen. Atelocollagen can be used to condense and deliver DNA, antisense oligodeoxynucleotides, virus vectors, and siRNAs into cells (27, 28).

Cells transfected with five genes, including neuronatin (Nnat), retinoblastoma 1 (Rb1), potassium channel subfamily K member 2 (TREK-1), ring finger protein 13 (Rnf13), and eukaryotic translation initiation factor 4A1 (eIF4A1), exhibited spontaneous neurite outgrowth. The morphologies of these transfected cells are shown in Fig. 2. Transfection of seven genes promoted cell growth. These growth-promoting genes were fibroblast growth factor (FGF)-inducible gene 14 (Fin14/Ddx3x), immediate-early response 2 gene (Ier2/pip92/ETR101), signal-induced proliferation-associated gene 1 (Sipa1/Spa1), Eph receptor A_3 (Epha3/Hek/Mek4), hepatoma-

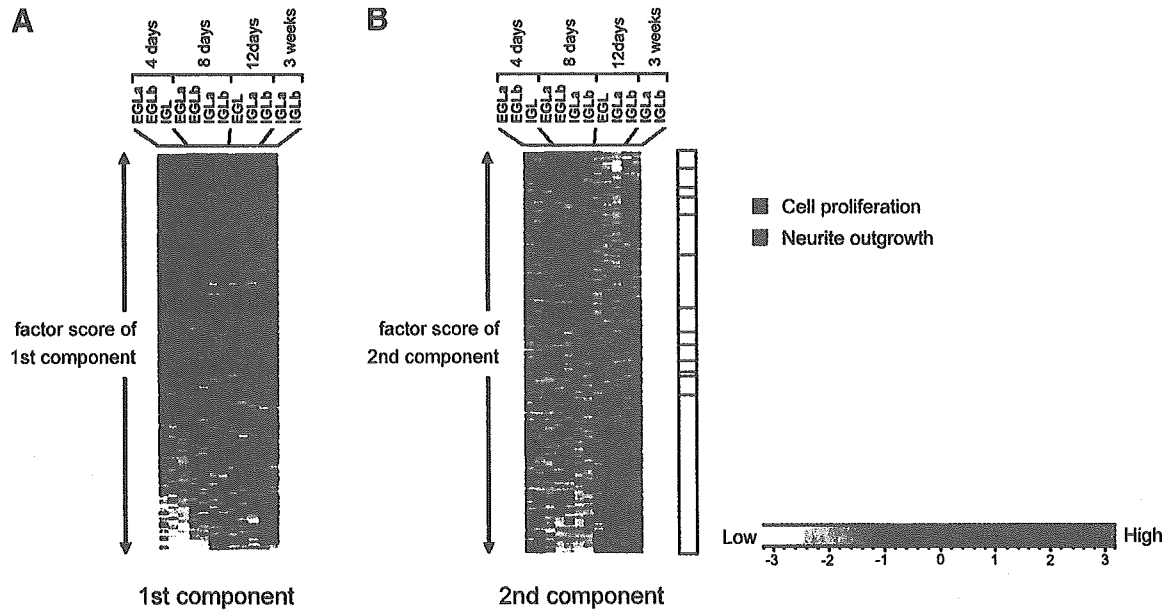

Fig. 1. Gene expression profiling during cerebellar granule cell differentiation; 450 genes (vertical axis) are arranged in order of the factor score of the first component (*A*) or the second component (*B*) of principal component analysis (PCA). Expression levels are indicated by color, with the scale shown at *bottom right*. Crossbars designate genes whose overexpression resulted in phenotypic changes (*B*). From *top* to *bottom*, blue bars (neurite outgrowth) indicate potassium channel subfamily K member 2 (TREK-1), retinoblastoma 1 (Rb1), ring finger protein 13 (Rnf13), eukaryotic translation initiation factor 4A1 (eIF4A1), and neuronatin (Nnat), and red bars (cell proliferation) indicate hepatoma-derived growth factor (Hdgf), fibroblast growth factor-inducible gene 14 (FIN14/Ddx3x), immediate-early response gene 2 (Ier2/pip92/ETR109), mitogen-activated protein kinase 6 (Mapk6/Erk3), Eph receptor A_3 (Epha3/Hek/Mek4), signal-induced proliferation-associated gene 1 (Sipa1/Spa1), Finkel-Biskis-Reilly murine sarcoma virus (FBR-MuSV) ubiquitously expressed gene (Fau/MNSFβ). EGLa, superficial area of the external granular layer (EGL); EGLb, internal area of the EGL; IGLa, internal granular layer (IGL) adjacent to the Purkinje cell layer; IGLb, internal area of the IGL.

derived growth factor (Hdgf), mitogen-activated protein kinase 6 (Mapk6/Erk3), and Finkel-Biskis-Reilly murine sarcoma virus (FBR-MuSV) ubiquitously expressed gene (Fau/MNSFβ).

Correlation between gene expression patterns and functions. To explore the relationship between gene expression and function, we aligned genes in the functional categories identified by the cell transfection array to the gene expression patterns sorted by the second component (Fig. 1*B*). The genes that functioned in neurite outgrowth and cell proliferation had characteristic distribution; none of these genes exhibited elevated expression at maturation. Figure 1*B* includes genes that were not analyzed in transfection experiments. In Fig. 3, the expression patterns of the 288 genes analyzed by transfection are shown in a more quantitative manner: the quantitative differences between the expression levels in 8-day and 12-day/3-week cerebella are plotted by the order of factor scores of the second component. There are no genes that functioned either in neurite outgrowth or cell proliferation distributed in the region where the indicator exhibited negative values.

We calculated the chance probability of the biased gene distribution. Because Nnat-3 is located nearest to the right end, we calculated the probability that all genes of a category are located on the left side of the Nnat-3 position. The *P* values for all genes, cell proliferation genes, and neurite outgrowth genes are 0.002, 0.028, and 0.267, respectively.

DISCUSSION

Identification of transcriptional activation or deactivation of functional gene classes would facilitate the understanding of molecular mechanisms underlying biological processes. Exploration of the correlations between gene expression patterns and functions has therefore been a central issue of transcriptome analysis. However, these analyses have usually been performed by subjective interpretation of individual scientists without valid evidence. Such arguments have often been based on previously published scientific literature rather than on information derived from the analysis of experimental systems. Experimental data regarding gene functions should provide more valid information. In this report, we described the simultaneous analysis of gene expression and function to test whether an expression-function correlation could be experimentally identified. One important finding herein is that none of the genes in the functional groups exhibited elevated expression at maturation. This result agrees with the gene expression-function correlation previously identified from the literature (20, 22). Taken together, these data imply that molecules that are functionally active in mature neurons are not likely to be active participants in the developmental process. Although confirmation with a larger number of genes is needed, our approach will provide a rigid basis for future studies of gene expression-function correlations.

The rat pheochromocytoma cell line PC12 is a well-characterized model for the study of neuron-like differentiation and signal transduction. There are many cases where genes involved in cerebellar development are induced phenotypic changes in PC12 cells. In response to expression of Wnt-1, a secreted signaling factor required for development of mammalian cerebellum, PC12 cells adopt a flat morphology reminiscent of epithelial cells, form extensive cell-cell contacts, and become refractory to neuronal differentiation induced by NGF (31). Moreover, NCAM, a member of the immunoglobulin

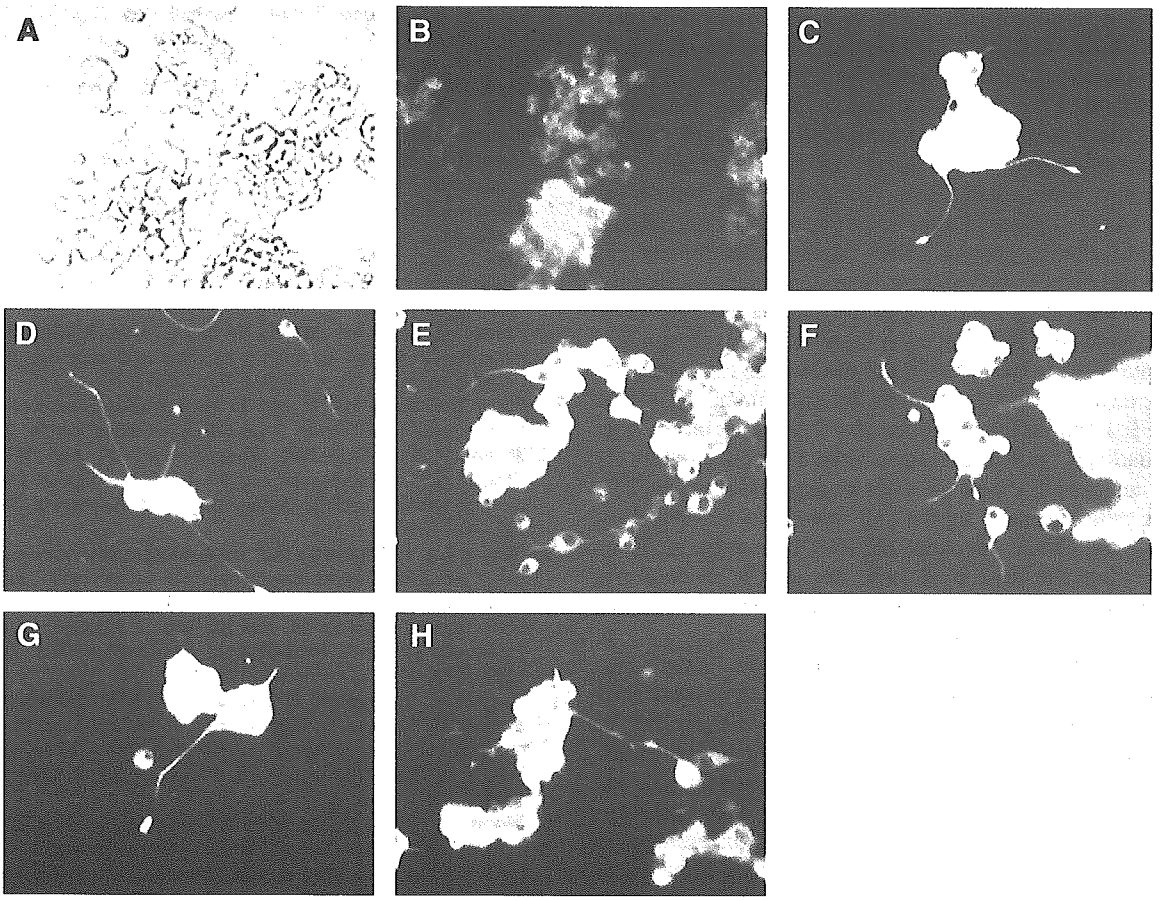

Fig. 2. Cell transfection array. PC12 cells transfected with enhanced green fluorescent protein alone (*A* and *B*) and PC12 cells differentiated into neurons by treatment with 100 ng/ml neuron growth factor (NGF; *C*). Fluorescent micrographs show neurite outgrowth of cells that overexpressed Nnat (*D*), Rb1 (*E*), TREK-1 (*F*), Rnf13 (*G*), and eIF4A1 (*H*) in the absence of NGF.

superfamily implicated in cerebellar granule cell migration, has stimulated neurite outgrowth from PC12 cells (8). Nnat protein is expressed much more highly in fetal and neonatal brains than in the adult brain (9) and is expressed in a segment-specific pattern during early hindbrain development (32), suggesting involvement in nervous system development. Rb1 is known to be a tumor suppresser gene and is hypophosphorylated in PC12 cells by NGF through the Ras signaling pathway (19). Hypophosphorylated Rb1 is essential for neurite outgrowth, as was demonstrated by inhibition with a monoclonal antibody against hypophosphorylated Rb (19). The related protein Rb2/p130 was reported to induce neurite outgrowth in the absence of NGF (29). Including our results, there is enough evidence to support the involvement of Rb1 in differentiation of PC12 cells. However, the role of Rb1 in cerebellar development is unknown. There have been very few reports of other genes that induced neurite outgrowth. Our findings should be a starting point for elucidating the roles of these genes in this process.

Most of the genes we identified as promoting cell growth have been described in the literature as having similar functions. Hdgf was found to have activity in hepatocytes (26) but may also be involved in nervous system development (1).

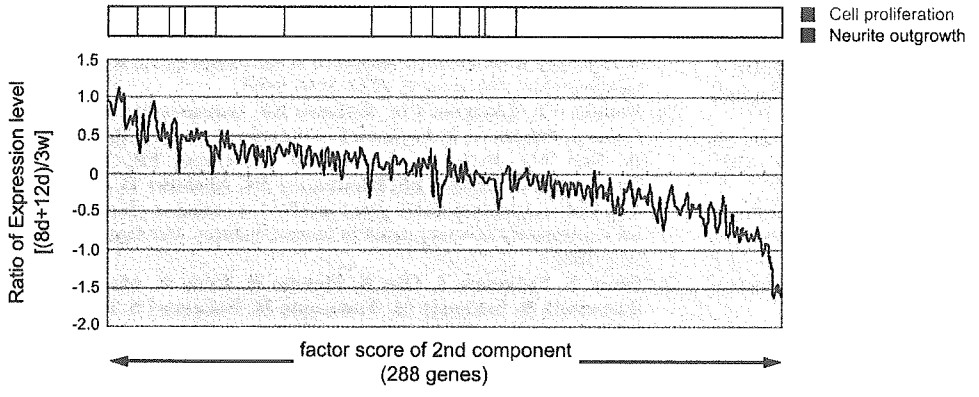

Fig. 3. The characteristics of the expression-function correlation. Vertical axis, the log-transformed ratio of the mean value of expression levels in 8-day cerebella to the mean value of expression levels in 12-day and 3-wk cerebella. Horizontal axis, the 288 genes subjected to transfection were sorted by the factor score of the second component of PCA. Crossbars designate genes whose overexpression resulted in phenotypic changes. From *left* to *right*, blue bars (neurite outgrowth) indicate TREK-1, Rb1, Rnf13, eIF4A1, and Nnat, and red bars (cell proliferation) indicate Hdgf, FIN14/Ddx3x, Ier2/pip92/ETR109, Mapk6/Erk3, Epha3/Hek/Mek4, Sipa1/Spa1, and Fau/MNSFβ.

Fin14/Ddx3x was initially identified as a FGF-inducible gene (14). Ier2/pip92/ETR101 was identified in FGF-stimulated hippocampal cells during neuronal differentiation (5) and in PC12 cells treated with cell proliferation agents, neuronal differentiation agents, and membrane depolarization agents (3). Sipa1/Spa1 is transcriptionally induced in murine lymphoid cells after mitogenic stimulation (15). The expression pattern of Epha3/Hek/Mek4 suggests its participation in guidance of cell migration and axonal growth cones during development (6, 12). Epha3/Hek/Mek4 displayed a lobe-dependent variability in expression pattern in the developing chick cerebellum (17), although its role in cerebellar development is poorly understood. Mapk6/Erk3 is localized in the nucleus in exponentially growing, quiescent, and growth factor-stimulated cells (4). Fau/MNSFβ, a lymphokine product of a T cell hybridoma, was originally isolated from a radiation-induced mouse osteosarcoma (11) and possibly acts as a tumor suppressor gene (23). Among the genes selected by the cell transfection assay, only a few genes, i.e., Nnat, Ier2/pip92/ETR101, and Epha3/Hek/Mek4, have direct evidence of gene expression in neuronal development. However, this does not exclude the possibility of other genes involvement in neuronal development.

There may be criticism that functionality in PC12 cells and cerebellar development are different biological processes. Thus activity in PC12 cells may not reflect processes occurring in cerebellar granule cells. However, another interpretation of our system is that this heterogeneity implies stringency of our experimental conditions: the genes we have identified are active enough to induce phenotypic changes in different types of cells, i.e., both PC12 and granule cells. The identification of functional genes depends on the assay system, and our current procedure is the most stringent as far as using this heterogeneous system. More sensitive assays such as transfection under weak stimulation by growth factors, e,g, NGF, may identify other genes. It should be noted that sensitive assays may increase pseudopositive hits, and it will be important to choose optimal conditions. Despite several reservations, we stress that the cell transfection array or comparable large-scale functional analysis is per se a strong approach to finding new molecules involved in a particular biological process.

GRANTS

This study was supported by the Program for Promotion of Fundamental Studies in Health Sciences of the Organization for Pharmaceuticals and Medical Devices Agency.

REFERENCES

1. **Abouzied MM, Baader SL, Dietz F, Kappler J, Gieselmann V, and Franken S.** Expression patterns and different subcellular localization of the growth factors HDGF (hepatoma-derived growth factor) and HRP-3 (HDGF-related protein-3) suggest functions in addition to their mitogenic activity. *Biochem J* 378: 169–176, 2004.
2. **Altman J and Bayer SA.** *Development of the Cerebellar System: In Relation to its Evolution, Structure, and Functions.* Boca Raton, FL: CRC 1996.
3. **Charles CH, Simske JS, O'Brien TP, and Lau LF.** Pip92: a short-lived, growth factor-inducible protein in BALB/c 3T3 and PC12 cells. *Mol Cell Biol* 10: 6769–6774, 1990.
4. **Cheng M, Boulton TG, and Cobb MH.** ERK3 is a constitutively nuclear protein kinase. *J Biol Chem* 271: 8951–8958, 1996.
5. **Chung KC, Shin SW, Yoo M, Lee MY, Lee HW, Choe BK, and Ahn YS.** A systemic administration of NMDA induces immediate early gene pip92 in the hippocampus. *J Neurochem* 75: 9–17, 2000.
6. **Connor RJ, Menzel P, and Pasquale EB.** Expression and tyrosine phosphorylation of Eph receptors suggest multiple mechanisms in patterning of the visual system. *Dev Biol* 193: 21–35, 1998.
7. **de Wildt RM, Mundy CR, Gorick BD, and Tomlinson IM.** Antibody arrays for high-throughput screening of antibody-antigen interactions. *Nat Biotechnol* 18: 989–994, 2000.
8. **Doherty P, Ashton SV, Moore SE, and Walsh FS.** Morphoregulatory activities of NCAM and N-cadherin can be accounted for by G protein-dependent activation of L- and N-type neuronal Ca^{2+} channels. *Cell* 67: 21–33, 1991.
9. **Dou D and Joseph R.** Cloning of human neuronatin gene and its localization to chromosome-20q 11.2–12: the deduced protein is a novel "proteolipid". *Brain Res* 723: 8–22, 1996.
10. **Falsey JR, Renil M, Park S, Li S, and Lam KS.** Peptide and small molecule microarray for high throughput cell adhesion and functional assays. *Bioconjug Chem* 12: 346–353, 2001.
11. **Finkel MP, Reilly CA Jr, and Biskis BO.** Pathogenesis of radiation and virus-induced bone tumors. *Recent Results Cancer Res* 54: 92–103, 1976.
12. **Flenniken AM, Gale NW, Yancopoulos GD, and Wilkinson DG.** Distinct and overlapping expression patterns of ligands for Eph-related receptor tyrosine kinases during mouse embryogenesis. *Dev Biol* 179: 382–401, 1996.
13. **Greene LA and Tischler AS.** Establishment of a noradrenergic clonal line of rat adrenal pheochromocytoma cells which respond to nerve growth factor. *Proc Natl Acad Sci USA* 73: 2424–2428, 1976.
14. **Guthridge MA, Seldin M, and Basilico C.** Induction of expression of growth-related genes by FGF-4 in mouse fibroblasts. *Oncogene* 12: 1267–1278, 1996.
15. **Hattori M, Tsukamoto N, Nur-e-Kamal MS, Rubinfeld B, Iwai K, Kubota H, Maruta H, and Minato N.** Molecular cloning of a novel mitogen-inducible nuclear protein with a Ran GTPase-activating domain that affects cell cycle progression. *Mol Cell Biol* 15: 552–560, 1995.
16. **Honma K, Ochiya T, Nagahara S, Sano A, Yamamoto H, Hirai K, Aso Y, and Terada M.** Atelocollagen-based gene transfer in cells allows high-throughput screening of gene functions. *Biochem Biophys Res Commun* 21: 1075–1081, 2001.
17. **Karam SD, Burrows RC, Logan C, Koblar S, Pasquale EB, and Bothwell M.** Eph receptors and ephrins in the developing chick cerebellum: relationship to sagittal patterning and granule cell migration. *J Neurosci* 20: 6488–6500, 2000.
18. **Kato K.** Adaptor-tagged competitive PCR: a novel method for measuring relative gene expression. *Nucleic Acids Res* 25: 4694–4696, 1997.
19. **Li H, Kawasaki H, Nishida E, Hattori S, and Nakamura S.** Ras-regulated hypophosphorylation of the retinoblastoma protein mediates neuronal differentiation in PC12 cells. *J Neurochem* 66: 2287–2294, 1996.
20. **Matoba R, Kato K, Kurooka C, Maruyama C, Sakakibara Y, and Matsubara K.** Correlation between gene functions and developmental expression patterns in the mouse cerebellum. *Eur J Neurosci* 12: 1357–1371, 2000.
21. **Matoba R, Kato K, Saito S, Kurooka C, Maruyama C, Sakakibara Y, and Matsubara K.** Gene expression in mouse cerebellum during its development. *Gene* 241: 125–131, 2000.
22. **Matoba R, Saito S, Ueno N, Maruyama C, Matsubara K, and Kato K.** Gene expression profiling of mouse postnatal cerebellar development. *Physiol Genomics* 4: 155–164, 2000.
23. **Michiels L, Van der Rauwelaert E, Van Hasselt F, Kas K, and Merregaert J.** fau cDNA encodes a ubiquitin-like-S30 fusion protein and is expressed as an antisense sequence in the Finkel-Biskis-Reilly murine sarcoma virus. *Oncogene* 8: 2537–2546, 1993.
24. **Mootha VK, Lindgren CM, Eriksson KF, Subramanian A, Sihag S, Lehar J, Puigserver P, Carlsson E, Ridderstrale M, Laurila E, Houstis N, Daly MJ, Patterson N, Mesirov JP, Golub TR, Tamayo P, Spiegelman B, Lander ES, Hirschhorn JN, Altshuler D, and Groop LC.** PGC-1alpha-responsive genes involved in oxidative phosphorylation are coordinately downregulated in human diabetes. *Nat Genet* 34: 267–273, 2003.
25. **Muro S, Takemasa I, Oba S, Matoba R, Ueno N, Maruyama C, Yamashita R, Sekimoto M, Yamamoto H, Nakamori S, Monden M, Ishii S, and Kato K.** Identification of expressed genes linked to malignancy of human colorectal carcinoma by parametric clustering of quantitative expression data. *Genome Biol* 4: R21, 2003.

26. **Nakamura H, Izumoto Y, Kambe H, Kuroda T, Mori T, Kawamura K, Yamamoto H, and Kishimoto T.** Molecular cloning of complementary DNA for a novel human hepatoma-derived growth factor. *J Biol Chem* 269: 25143–25149, 1994.
27. **Ochiya T, Takahama Y, Nagahara S, Sumita Y, Hisada A, Itoh H, Nagai Y, and Terada M.** New delivery system for plasmid DNA in vivo using atelocollagen as a carrier material: the minipellet. *Nat Med* 5: 707–710, 1999.
28. **Ochiya T, Nagahara S, Sano A, Itoh H, and Terada M.** Biomaterials for gene delivery: atelocollagen-mediated controlled release of molecular medicines. *Curr Gene Ther* 1: 31–52, 2001.
29. **Paggi MG, Bonetto F, Severino A, Baldi A, Battista T, Bucci F, Felsani A, Lombardi D, and Giordano A.** The retinoblastoma-related Rb2/p130 gene is an effector downstream of AP-2 during neural differentiation. *Oncogene* 20: 2570–2578, 2001.
30. **Saito S, Matoba R, and Kato K.** Adapter-tagged competitive PCR (ATAC-PCR)–a high-throughput quantitative PCR method for microarray validation. *Methods* 31: 326–331, 2003.
31. **Shackleford GM, Willert K, Wang J, and Varmus HE.** The Wnt-1 proto-oncogene induces changes in morphology, gene expression, and growth factor responsiveness in PC12 cells. *Neuron* 11: 865–875, 1993.
32. **Wijnholds J, Chowdhury K, Wehr R, and Gruss P.** Segment-specific expression of the neuronatin gene during early hindbrain development. *Dev Biol* 171: 73–84, 1995.
33. **Ziauddin J and Sabatini DM.** Microarrays of cells expressing defined cDNAs. *Nature* 411: 107–110, 2001.

Cell Transplantation, Vol. 14, pp. 629–635, 2005

0963-6897/05 $20.00 + .00
E-ISSN 1555-3892
www.cognizantcommunication.com

Long-Term Maintenance of Liver-Specific Functions in Cultured ES Cell-Derived Hepatocytes With Hyaluronan Sponge

Takumi Teratani,* Gary Quinn,* Yusuke Yamamoto,*† Tomoya Sato,‡ Hiroko Yamanokuchi,‡ Akira Asari,‡ and Takahiro Ochiya*

*National Cancer Center Research Institute, 1-1, Tsukiji, 5-chome, Chuo-ku, Tokyo 104-0045, Japan
†Department of Biology, School of Education, Waseda University, Tokyo 169-0051, Japan
‡Central Research Laboratories, Seikagaku Corporation, 1253 Tateno 3-chome, Higashiyamato-shi, Tokyo 207-0021, Japan

This study investigated the three-dimensional culture of hepatocytes differentiated from mouse embryonic stem (ES) cells with a porous hyaluronan (HA) sponge support. Hepatocytes were immobilized within the pores of the support. Spheroids could be observed within the support, each containing between 20 and 50 hepatocytes. To examine the liver-specific functions of the hepatocytes in the culture, the levels of albumin secreted into the medium were analyzed. The secretion of albumin was stable over the course of 32 days, longer than that in both conventional monolayer and collagen sponge cultures. To elucidate further the liver-specific functions of hepatocytes embedded in the HA sponge, metabolic activities of the hepatocytes were examined for their ability to eliminate ammonia from culture media and the synthesis of urea nitrogen. While rates of ammonia removal and urea nitrogen synthesis were similar to those in both conventional monolayer and in collagen sponge cultures, these functions were maintained for longer duration in cells embedded in the HA sponge. These results demonstrate that the porous HA sponge is an effective support for the in vitro culture of ES-derived hepatocytes used for both basic and applied studies for cell transplantation.

Key words: Embryonic stem cells; Hepatocytes; Hyaluronan (HA) sponge; Three-dimensional; Spheroid

INTRODUCTION

ES cells were first identified in the mouse system and are capable of differentiating in vitro into multiple cell types (22). In the past decade, several growth factors and transcription factors have been shown to be capable of directing differentiation of mouse ES cells into multicell lineages in vitro; for example, retinoic acid induces neurons (6); cytokines induce hematopoietic cells (7,30); fibroblast growth factors induce hematopoietic cells (4); transforming growth factor induces myogenesis (25); and hepatic nuclear factor (HNF)-3 induces endoderm cells. ES cells cultured on several different feeder cell layers are also induced to differentiate into specific cell types (16,17). Recently, insulin-secreting pancreatic islet-like cells were isolated from the endoderm of differentiated ES cells (13). Hence, ES cells will provide a powerful tool for studying differentiation and function of various cell types. Furthermore, this apparent "plasticity" of stem cells has become a holy grail of stem cell therapeutics, promising the eventual clinical use of embryonic stem cells in the regeneration of damaged tissues. Recently, differentiation of hepatocytes from ES cells in vitro (8,10,31) and in vivo (1,2) has been reported. However, none of the previous work with ES cells revealed an efficient differentiation into functional hepatocytes or any therapeutic application. We have reported for the first time that ES cells can differentiate into hepatic cells after adoptive transfer into liver-injured mouse recipients (32). Using albumin promoter-induced GFP expression, morphological features, and immunohistochemical analyses of hepatocyte specific markers, we have demonstrated that ES cells are capable of producing hepatocytes. In our estimation, 2×10^6 ES cells differentiated into approximately 3×10^7 hepatocytes. These ES cell-derived hepatocytes are transplantable into animals; they express liver functions and ameliorate liver injury, indicating that they could provide a source of cell therapies for the treatment of liver disease.

In the development of stem cell-derived hepatocyte-based therapies, a suitable microenvironment for cells still needs to be developed to provide the long-term maintenance of liver-specific functions and liver-specific gene expression in the hepatocytes. To date, many artifi-

Address correspondence to Takahiro Ochiya, Ph.D., Head of Section for Studies on Metastasis, National Cancer Center Research Institute, 1-1, Tsukiji 5-chome, Chuo-ku, Tokyo 104-0045, Japan. Tel: 81-3-3542-2511; Fax: 81-3-3541-2685; E-mail: tochiya@ncc.go.jp

cial liver systems have been investigated by many researchers, including hydrogel microspheres, hollow fibers, and macroporous polymer scaffolds. In addition, hepatocytes cultured on highly porous biocompatible as well as biodegradable polymers have been utilized for long-term maintenance of hepatocytes. In most cases, researchers have focused on three-dimensional scaffolds such as poly(lactide-*co*-glycolide) (9,11), polyurethane (23), collagen (26,27), chitosan (3), alginate (5), and hydrogel (20,21). Thus, selecting the material for such a scaffold is critically important for the success of potential ES-based cell therapy for amelioration of liver injury. Our group has recently developed a porous scaffold based on hyaluronan (HA) (T. Sato et al., Seikagaku Corp., Tokyo, Japan). In the present article, we characterize the three-dimensional culture of hepatocytes derived from mouse ES cells with a porous HA sponge support. The results presented in this study indicate that the porous HA sponge is an effective support for the long-term in vitro culture of hepatocytes, and a promising substrate for future bioartificial liver design and for applied studies on ES cell-based cell therapy.

MATERIALS AND METHODS

Culture of ES Cells

pALB-EGFP/ES cells, carrying the pALB-EGFP construct (19), were cultured to maintain pluripotency on STO feeder cells with 1000 U/ml LIF/ESGRO (Amrad) in ES cell culture medium. pALB-EGFP was consisted of mouse albumin promoter/enhancer and EGFP vector. Once hepatic differentiation occurred, the albumin expressing cells were identified as green fluorescent protein (GFP) positive. GFP gene expression was monitored by fluorescence microscopy.

Hepatic Induction From ES Cells In Vivo

The pALB-EGFP/ES cells were cultured in LIF(\min\) culture medium for 24 h before injecting into the animals. There were no GFP-positive cells detectable in the preculture of ES cells as determined by fluorescence microscopy. Twenty-four hours prior to cell injection, male 10-week-old 129SVJ mice were treated with an intraperitoneal injection of carbon tetrachloride (CCl_4). Mice administered with olive oil alone were used as a control. All of these mice were then injected with 2×10^6 ES cells intravenously through the tail vein. ES cells were differentiated in vivo in the form of teratomas. GFP gene expression was monitored by fluorescence microscopy.

In Vitro Monolayer Culture

GFP-positive fractions were washed with cold PBS(–) three times and the tissues were cut with scissors into approximately 1.0-mm^3 pieces. These were then transferred into a new tube and gently stirred for 20 min at 37°C in PBS containing 0.05% collagenase (GIBCO-BRL) and 1000 U/ml dispase (Godoshusei Co., Tokyo, Japan). The dissociated cells were washed twice with serum-free DMEM and then resuspended in hepatocyte culture medium (modified William E medium) containing transferrin (5 μg/ml), hydrocortisone-21-hemisuccinate (10^{-6} M), bovine serum albumin (0.5 mg/ml), ascorbic acid (2 mM), insulin (5 μg/ml), and gentamicin (50 μg/ml) (Sanko Junyaku Co., Ltd., Tokyo, Japan). Two days after plating, fresh medium containing 10 mM niacinamide, 10^{-6} M dexamethasone and 175 μg/ml G418 was added. The cells were cultured on collagen-coated plates (Koken Co. Ltd., Tokyo, Japan) and used for further studies. The same culture medium was used for the culturing of hepatocytes in HA and collagen sponge.

Culturing of Hepatocytes in a HA Sponge

To obtain a three-dimensional culture, viable GFP-positive hepatocytes were seeded into a porous 10-mm-square × 1.0-mm-thick photo-cross-linked HA sponge that includes cinnamic acid as a cross-linking material (Seikagaku Corp., Tokyo, Japan) maintained in a 24-well plate at a density of 2×10^7 cells/ sponge. The hepatocytes were cultured in the culture medium described above with 1.0 ml/well. The sponge cultures were compared with monolayer cultures of the same number of GFP-positive hepatocytes on culture plates coated with type I collagen or three-dimensional culture embedded in collagen sponge (Koken Co. Ltd., Tokyo, Japan).

Biochemical Analyses of ES Cell-Derived Hepatocytes

One day after embedding in the HA sponge, GFP-positive hepatocytes, control ES cells, and normal mouse hepatocytyes were analyzed for glucose levels in culture supernatant by the glucose oxidase method, as described previously (24). The release of albumin into the culture medium was measured by ELISA (32) every 3 days. To compare cellular activity of ammonia detoxification, GFP-positive hepatocytes in the HA sponge, in collagen-coated plate, and in collagen sponge were cultured in DMEM containing 2.5 mM NH_4Cl and further incubated for 24 h. Culture media were tested for NH_4Cl concentration at 0, 6, 12, and 24 h by Ammonia-Test Wako (Wako Pure Chemicals Co., Ltd., Japan). To determine the urea synthesis ability, cells were cultured with HBSS in the presence of 5 mmol/L NH_4Cl. The medium was harvested after incubation for 0, 2, 4, and 6 h and subjected to assay according to the described method. As a control, primary cultured mouse hepatocytes embedded in HA sponge were used.

Statistical Analysis

Results are given as mean ± SD. The Student's *t*-test was performed for statistical evaluation, with $p < 0.05$ considered significant.

RESULTS

Preparation of Hepatocytes From ES Cells

pALB-EGFP/ES cells were injected into 129SVJ mice pretreated with CCl_4. CCl_4-treated mice provide a liver regeneration environment that might present multiple growth factors and cytokines to assist hepatic cell generation and hepatic cell induction. Tumor formation was observed in the liver of all CCl_4-treated mice, whereas no tumors were detected in the control mice without CCl_4 administration. The tumors were analyzed by fluorescence microscopy, which revealed the presence of GFP-positive fractions, indicative of differentiated hepatocytes marked by the lineage-tracing pALB-EGFP construct. These GFP-positive fractions, comprising approximately 30% of total tumor volumes, were dissected and the GFP-positive cells harvested by enzymatic digestion; 98% of harvested cells were GFP positive.

Hepatocyte Characteristics of GFP-Positive Cells

ES cell-derived GFP-positive cells can be cultured in vitro with a typical hepatocyte morphology (Fig. 1). In addition, GFP-positive cells were immunohistochemically positive for albumin, alpha-1-antitrypsin, and transferrin (data not shown). RT-PCR analysis revealed that cultured GFP-positive cells were positive for several hepatocyte-specific markers including albumin, tryptophan 2,3-dioxygenase, alpha-1-antitryspin, and transthyretin (data not shown). Liver-specific transcription factors including HNFs were also detected in GFP-positive cells (data not shown).

Properties of ES Cell-Derived Hepatocytes Embedded in the Hyaluronic Acid Sponge

Following enzymatic digestion of the GFP-positive fractions, cells were resuspended in hepatocyte culture medium containing several hepatocyte growth factors. Addition of G418 to the medium served to exclude host-derived hepatocytes from the culture. Following 3 days in culture on collagen-coated plates, about 5×10^7 GFP-positive cells with 97% viability were obtained from 2×10^6 ES cells injected into the mouse in a typical experiment. Two milliliters of cell suspension containing 1.0×10^7 cells/ml was soaked into the HA sponge (10-mm square × 1.0-mm thickness) (Fig. 2A) and incubated for 3 h. Next, 1.0 ml of culture medium was added for further culturing. The trypan blue exclusion test revealed that more than 90% of the embedded cells were viable after incubation for 20 days. As shown in Figure 2B, GFP-positive cells formed multicellular spheroids in the reticulated pores. Histochemical analysis showed that these multicellular spheroids contained 20–50 hepatocytes (Fig. 2C).

Metabolic Activity of Cultured Hepatocytes

To further elucidate whether GFP-positive cells embedded in the HA sponge displayed hepatocyte-specific functions, we performed biochemical analyses. Our results indicate that hepatic glucose production was significantly greater for cells in the HA sponge (0.079 ± 0.004 mmol/ml/h/10^4 cells, $n = 4$) compared with cells on collagen-coated plates (0.048 ± 0.003 mmol/ml/h/10^4 cells, $n = 4$) or in collagen sponge (0.057 ± 0.006 mmol/ml/h/10^4 cells, $n = 4$) 24 h after culturing. The cells embedded

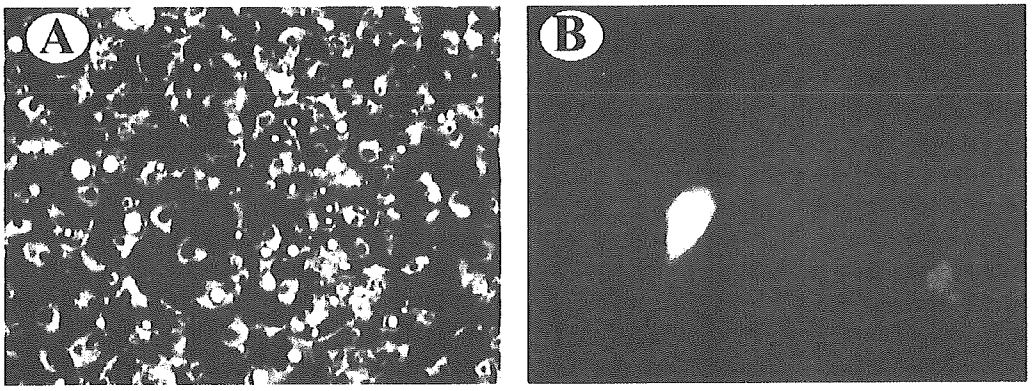

Figure 1. Phase-contrast photographs of ES cell-derived hepatocytes. GFP-positive fractions were digested with enzymes and cultured for 3 days on collagen-coated plates. (A) Cultured cells revealed hepatocyte-like morphology with a mononuclear, polyhedral structure and were arranged in trabeculae. (B) The same cells of (A) retained GFP positivity.

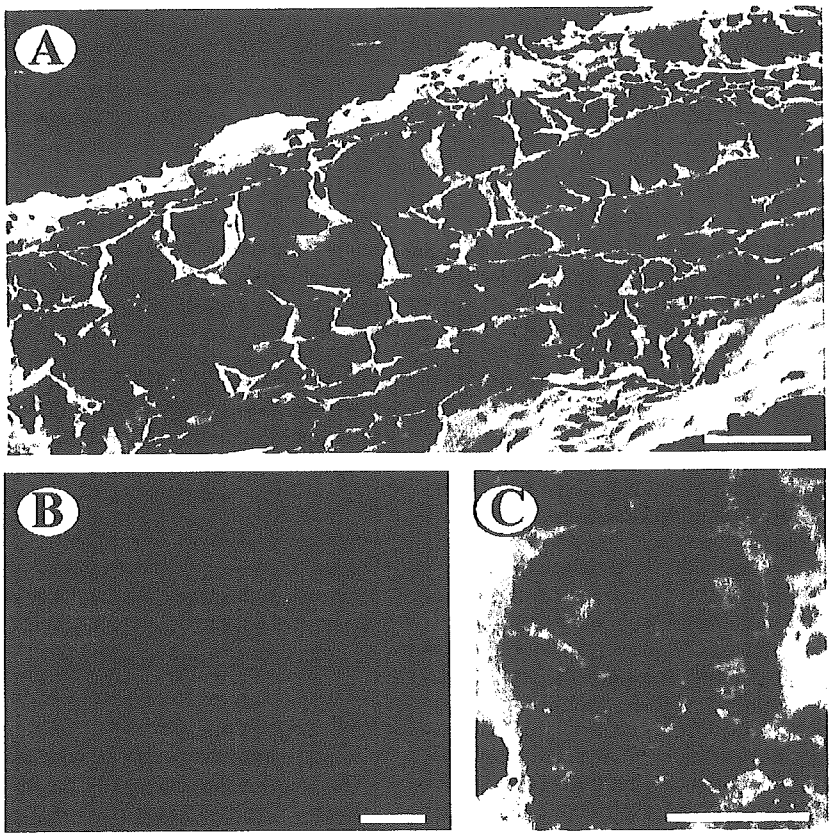

Figure 2. ES cell-derived hepatocytes embedded into a HA sponge. (A) Scanning electron microphotograph of the HA sponge is shown. The spongy matrix has a unique structure composed of a hyaluronic acid layer with large porous structure. Scale bar: 100 μm. (B) GFP-positive cells formed multicellular speroids in the reticulated pores. Scale bar: 50 μm. (C) The multicellular speroids were stained with May-Giemsa solution. Scale bar: 50 μm.

in HA sponge displayed relatively high albumin-producing ability (Fig. 3), whereas cells embedded in collagen sponge or monolayer cultures on collagen plates for the same period produced significantly lower levels of albumin. Hepatocytes embedded in the HA sponge retained hepatocyte functions for more than 20 days in culture, whereas control cells cultured on collagen plates or collagen sponge lost these functions after day 17. Albumin producing ability of cells in the HA sponge was observed for 32 days and thereafter was lost. Hepatocytes embedded in the HA sponge also secreted ureanitorogen (Fig. 4A) and were able to clear ammonia from the culture medium (Fig. 4B). Urea formation and ammonia elimination activities were also maintained for prolonged periods up to 20 days, indicating that the HA sponge effectively extends hepatocyte function in vitro. These results demonstrate that hepatocytes differentiated from ES cells retain hepatocyte characteristics including metabolic activities for prolonged time periods when embedded into the HA sponge.

DISCUSSION

Recent reports have highlighted the differentiation of hepatocytes from ES cells in vitro and in vivo. Cell transplantation strategies have been one major approach for overcoming organ transplantation. Although the transplantation of mature human hepatocytes will be the most promising scenario, primary cultured hepatocytes are not appropriate because they are difficult to prepare. Alternatively, human ES cell-derived hepatocytes will be a strong candidate for this procedure. However, none of the articles has demonstrated the long-term maintenance of ES cell-derived hepatocytes in vitro for further analysis of liver-specific function suitable for cell therapies. To address this question, we established the three-dimensional culture of ES cell-derived hepatocytes using a HA sponge. The HA sponge-embedded cells display the characteristics of mature hepatocytes with respect to liver-specific gene expression and functionality in vitro. Our novel culture system will be a valuable tool for

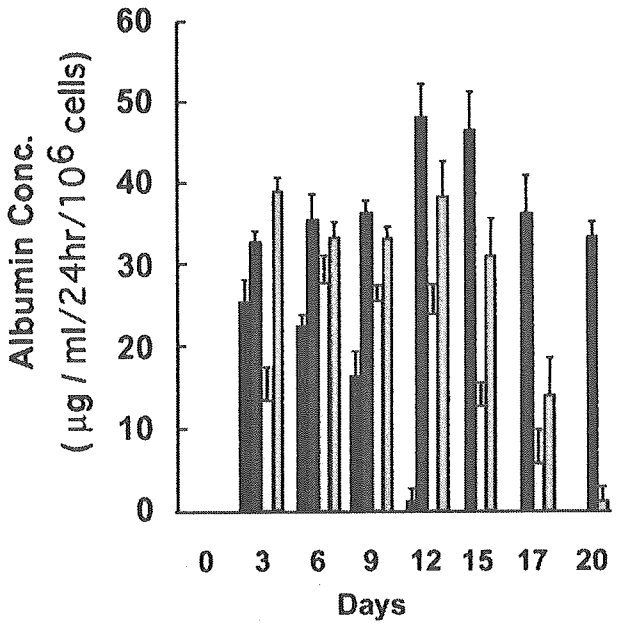

Figure 3. Albumin-producing ability of ES cell-derived hepatocytes cultured in the HA sponge. GFP-positive cells in HA sponge were analyzed for albumin levels in culture supernatant by ELISA (dark shaded columns) every 3 days and data are represented as μg/ml/24 h/10^6 cells. As controls, monolayer culture on collagen plates (black columns) and a collagen sponge (white columns) were used. Albumin-producing ability of the primary cultured mouse hepatocytes embedded in HA sponge was also assessed (light shaded columns). Data are represented as mean ± SD ($n = 6$).

studying the molecular and cellular basis of hepatic cells derived from stem cells in vitro and provide a potential basis for stem cell therapies to treat hepatic failure in vivo.

On collagen-coated dishes, primary cultured mouse hepatocyte monolayers stopped secreting albumin within 10 days. Our results suggest that the maintenance of albumin secretion by the ES cell-derived hepatocytes in monolayer culture is similar to that of primary culture of mouse hepatocytes. However, when cells were embedded into the HA sponge, the albumin-secreting abilities were greatly prolonged and the effect was much enhanced compared with collagen sponge. It has been reported that the high maintenance of albumin secretion by the hepatocytes in sponge culture is due to spheroid formation (23,33). However, the spheroid formation was much enhanced when the hepatocytes were embedded in the HA sponge compared with collagen sponge. These results suggest that efficient spheroid formation is a key factor for long-term maintenance of functions of ES-derived hepatocytes.

Hyaluronan, an abundant nonsulfated glycosaminoglycan component of synovial fluid and extracellular matrices, is an attractive biomaterial for design of new biocompatible and biodegradable polymers that have applications in drug delivery, wound healing, surgical adhesions, and tissue engineering (15). It is well known that in organogenesis and tissue regeneration, hyaluronan plays a crucial role in cell behavior: mesenchymal cells invading the primary corneal stroma to form the mature cornea; neural crest cells traveling from the neural tube to form ganglia of the peripheral nervous system; sclerotomal cells approaching and surrounding the notochord to form vertebrae; cushion cells migrating from the endocardium towards the myocardium during formation of heart valves; neuronal and glial precursors moving and proliferating during brain development; mesenchymal cells dividing and migrating during embryonic limb development, salamander limb regeneration, tendon regeneration, and fetal wound repair; and tumor cell growth and invasion (28,29). A variety of chemical modifications of native HA have been devised to provide mechanically and chemically robust materials. The resulting HA derivatives have physicochemical properties that may significantly differ from the native polymer, but most derivatives retain the biocompatibility and biodegradability. With our HA sponge, high-density hepatocytes can be maintained inside the pores, allowing three-dimensional cell to cell contact. These scaffolds should allow the cultivation of a large cell mass, the rearrangement of dispersed cells into a functioning tissue, and, following implantation, they may enable close interaction and metabolite transfer between the transplanted tissue and the host.

Among various methods developed for treating severe acute liver failure, only whole-liver transplantation has proven clinically useful. However, liver transplantation carries problems such as organ rejection and limited availability of donor livers. Although porcine xenotransplantation may be a promising alternative to liver allotransplantation, major immunological hurdles have yet to be overcome and, additionally, porcine endogenous retroviruses pose a safety concern (18). Recent progress in stem cell research should allow for the use of patients' own stem cell-derived hepatocytes, and engineered hepatocyte cell transplantation represents an alternative strategy for treating acute liver disease (12,14). In this regard, our novel approach for long-term maintenance of ES-derived hepatocytes with a HA sponge might be applicable for developing clinical grade hepatocytes from stem cells such as human ES cells and mesenchymal stem cells for cell therapy.

In summary, we found that the HA sponge, with a hydrophilic surface and reticulated structure, formed hepatocyte spheroids within its pores. Furthermore, specific interaction between the hepatocytes and the HA substrate appears to enhance the rate of spheroid formation. A three-dimensional HA sponge has features con-

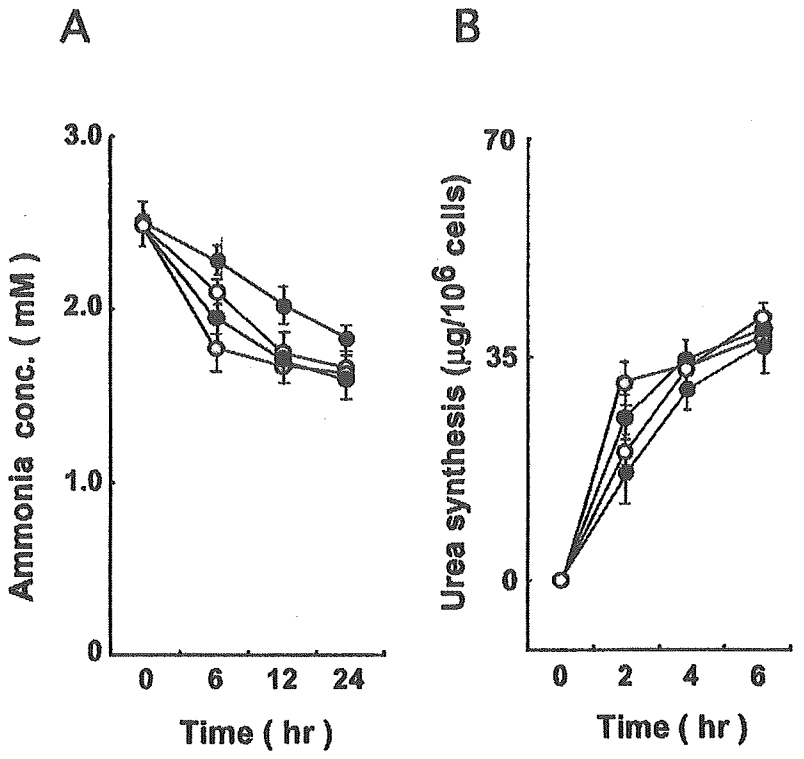

Figure 4. Urea release and ammonia elimination by ES-derived hepatocytes in the HA sponge. One day after plating, GFP-positive cells embedded in HA sponge (dark shaded circles) were examined for their potential to release urea into the culture medium (A) and eliminate ammonia from culture media (B). As controls, monolayer culture on collagen plates (black circles) and a collagen sponge (white circles) were used. As a control, primary cultured mouse hepatocytes embedded in HA sponge (light shaded circles) were used. Data are represented as mean ± SD ($n = 6$).

ducive to obtaining high cell density, and to sustaining cell viability and liver functions, over prolonged time periods when compared with a conventional monolayer culture or collagen-based sponge.

ACKNOWLEDGMENTS: We thank Ms. Ayako Inoue, Ms. Kazumi Kimura, Ms. Kimi Honma, Ms. Manami Ando, Ms. Maho Kodama, and Ms. Masako Hosoda for their excellent technical assistance. This work was supported in part by a Grant-in-Aid for the 3rd-Term Comprehensive 10-Year Strategy for Cancer Control; Health Science Research Grants for Research on the Human Genome and Gene Therapy from the Ministry of Health, Labour, and Welfare of Japan; and the Program for Promotion of Fundamental Studies in Health Sciences of the Organization for Pharmaceutical Safety and Research of Japan.

REFERENCES

1. Chinzei, R.; Tanaka, Y.; Shimizu-Saito, K.; Hara, Y.; Kakinuma, S.; Watanabe, M.; Teramoto, K.; Arii, S.; Takase, K.; Sato, C.; Terada, N.; Teraoka, H. Embryoid-body cells derived from a mouse embryonic stem cell line show differentiation into functional hepatocytes. Hepatology 36:22–29; 2002.
2. Choi, D.; Oh, H. J.; Chang, U. J.; Koo, S. K.; Jiang, J. X.; Hwang, S. Y.; Lee, J. D.; Yeoh, G. C.; Shin, H. S.; Lee, J. S.; Oh, B. In vivo differentiation of mouse embryonic stem cells into hepatocytes. Cell Transplant. 11:359–368; 2002.
3. Elcin, Y. M.; Dixit, V.; Gitnick, G. Hepatocyte attachment on biodegradable modified chitosan membranes: In vitro evaluation for the development of liver organoids. Artif. Organs 22:837–846; 1998.
4. Faloon, P.; Arentson, E.; Kazarov, A.; Deng, C. X.; Porcher, C.; Orkin, S.; Choi, K. Basic fibroblast growth factor positively regulates hematopoietic development. Development 127:1931–1941; 2000.
5. Glicklis, R.; Shapiro, L.; Agbaria, R.; Merchuk, J. C.; Cohen, S. Hepatocyte behavior within three-dimensional porous alginate scaffolds. Biotechnol. Bioeng. 67:344–353; 2000.
6. Gottlieb, D. I.; Huettner, J. E. An in vitro pathway from embryonic stem cells to neurons and glia. Cells Tissues Organs 165:165–172; 1999.
7. Gutierrez-Ramos, J. C.; Palacios, R. In vitro differentiation of embryonic stem cells into lymphocyte precursors able to generate T and B lymphocytes in vivo. Proc. Natl. Acad. Sci. USA 89:9171–9175; 1992.
8. Hamazaki, T.; Iiboshi, Y.; Oka, M.; Papst, P. J.; Meacham, A. M.; Zon, L. I.; Terada, N. Hepatic maturation in differentiation embryonic stem cell in vitro. FEBS Lett. 497:15–19; 2001.

9. Hasirci, V.; Berthiaume, F.; Bondre, S. P.; Gresser, J. D.; Trantolo, D. J.; Toner, M.; Wise, D. L. Expression of liver-specific functions by rat hepatocytes seeded in treated poly(lactic-co-glycolic) acid biodegradable foams. Tissue Eng. 7:385–394; 2001.
10. Jones, E. A.; Tosh, D.; Wilson, D. I.; Lindsay, S.; Forrester, L. M. Hepatic differentiation of murine embryonic stem cells. Exp. Cell Res. 272:15–22; 2002.
11. Kaufmann, P. M.; Heimrath, S.; Kim, B. S.; Mooney, D. J. Highly porous polymer matrices as a three-dimensional culture system for hepatocytes. Cell Transplant. 6: 463–468; 1997.
12. Kobayashi, N.; Miyazaki, M.; Fukaya, K.; Inoue, Y.; Sakaguchi, M.; Noguchi, H.; Matsumura, T.; Watanabe, T.; Totsugawa, T.; Tanaka, N.; Namba, M. Treatment of surgically induced acute liver failure with transplantation of highly differentiated immortalized human hepatocytes. Cell Transplant. 9:733–735; 2000.
13. Lumelsky, N.; Blondel, O.; Laeng, P.; Velasco, I.; Ravin, R.; McKay, R. Differentiation of embryonic stem cells to insulin-secreting structures similar to pancreatic islets. Science 292:1389–1394; 2001.
14. Malhi, H.; Gupta, S. Hepatocyte transplantation: new horizons and challenges. J. Hepatobil. Pancreat. Surg. 8:40–50; 2001.
15. McDonald, J. A.; Camenisch, T. D. Hyaluronan: Genetic insights into the complex biology of a simple polysaccharide. Glycoconj. J. 19:331–339; 2002.
16. Nakano, T.; Kodama, H.; Honjo, T. In vitro development of primitive and definitive erythrocytes from different precursors. Science 272:722–724; 1996.
17. Palacios, R.; Golunski, E.; Samaridis, J. In vitro generation of hematopoietic stem cells from an embryonic stem cell line. Proc. Natl. Acad. Sci. USA 92:7530–7534; 1995.
18. Patience, C.; Takeuchi, Y.; Weiss, R. A. Infection of human cells by an endogenous retrovirus of pigs. Nat. Med. 3:282–286; 1997.
19. Quinn, G.; Ochiya, T.; Terada, M.; Yoshida, T. Mouse flt-1 promoter directs endothelial-specific expression in the embyroid body model of embryogenesis. Biochem. Biophys. Res. Commun. 276:1089–1099; 2002.
20. Risbud, M. V.; Karamuk, E.; Moser, R.; Mayer, J. Hydrogel-coated textile scaffolds as three-dimensional growth support for human umbilical vein endothelial cells (HUVECs): Possibilities as coculture system in liver tissue engineering. Cell Transplant. 11:369–377; 2002.
21. Risbud, M.; Karamuk, E.; Schlosser, V.; Mayer, J. Hydrogel-coated textile scaffolds as candidate in liver tissue engineering: II. Evaluation of spheroid formation and viability of hepatocytes. J. Biomater. Sci. Polym. Ed. 14: 719–731; 2003.
22. Robertson, E. J. Teratocarcinoma and embryonic stem cells. In: Robertson, E. J., ed. A practical approach. Washington, DC: IRL Press; 1987:71–112.
23. Sato, Y.; Ochiya, T.; Yasuda, Y.; Matsubara, K. A new three-dimensional culture system for hepatocytes using reticulated polyurethane. Hepatology 19:1023–1028; 1994.
24. Sistare, F. D.; Haynes, Jr., R. C. The interaction between the cytosolic pyridine nucleotide redox potential and gluconeogenesis from lactate/pyruvate in isolated rat hepatocytes. Implications for investigations of hormone action. J. Biol. Chem. 260:12748–12753; 1985.
25. Slager, H. G.; Van Inzen, W.; Freund, E.; Van den Eijnden-Van Raaij, A. J.; Mummery, C. L. Transforming growth factor-beta in the early mouse embryo: Implications for the regulation of muscle formation and implantation. Dev. Genet. 14:212–224; 1993.
26. Takeshita, K.; Ishibashi, H.; Suzuki, M.; Yamamoto, T.; Akaike, T.; Kodama, M. High cell-density culture system of hepatocytes entrapped in a three-dimensional hollow fiber module with collagen gel. Artif. Organs 19:191–193; 1995.
27. Takimoto, Y.; Dixit, V.; Arthur, M.; Gitnick, G. De novo liver tissue formation in rats using a novel collagen-polypropylene scaffold. Cell Transplant. 12:413–421; 2003.
28. Toole, B. P. Glycosaminoglycans in morphogenesis. In: Hay, E., ed. Cell biology of extracellular matrix. New York: Plenum Press; 1981:259–294.
29. Toole, B. P. Proteoglycans and hyaluronan in morphogenesis and differentiation. In: Hay, E., ed. Cell biology of extracellular matrix, 2nd ed. New York: Plenum Press; 1991:305–341.
30. Wiles, M. V.; Keller, G. Multiple hematopoietic lineages develop from embryonic stem (ES) cells in culture. Development 111:259–267; 1991.
31. Yamada, T.; Yoshikawa, M.; Kanda, S.; Kato, Y.; Nakajima, Y.; Ishizaka, S.; Tsunoda, Y. In vitro differentiation of embryonic stem cells into hepatocytes-like cells identified by cellular uptake of indocyanine green. Stem Cells 20:146–154; 2002.
32. Yamamoto, H.; Quinn, G.; Asari, A.; Yamanokuchi, H.; Teratani, T.; Terada, M.; Ochiya, T. Differentiation of embryonic stem cells into hepatocytes: Biological functions and therapeutic application. Hepatology 37:983–993; 2003.
33. Yamashita, Y.; Shimada, M.; Tsujita, E.; Shirabe, K.; Ijima, H.; Nakazawa, K.; Sakiyama, R.; Fukuda, J.; Funatsu, K.; Sugimachi, K. High metabolic function of primary human and porcine hepatocytes in a polyurethane foam/spheroid culture system in plasma from patients with fulminant hepatic failure. Cell Transplant. 11:379–384; 2002.

Recapitulation of *In Vivo* Gene Expression During Hepatic Differentiation From Murine Embryonic Stem Cells

Yusuke Yamamoto,[1,2] Takumi Teratani,[1] Hanako Yamamoto,[3] Gary Quinn,[1] Sigenori Murata,[4] Rieko Ikeda,[4] Kenji Kinoshita,[4] Kenichi Matsubara,[4] Takashi Kato,[2] and Takahiro Ochiya[1]

Hepatic differentiation at the molecular level is poorly understood, mainly because of the lack of a suitable model. Recently, using adherent monoculture conditions, we demonstrated the direct differentiation of hepatocytes from embryonic stem (ES) cells. In this study, we exploited the direct differentiation model to compare the gene expression profiles of ES cell–derived hepatocytes with adult mouse liver using DNA microarray technology. The results showed that the ES cell–derived hepatocyte gene expression pattern is very similar to adult mouse liver. Through further analysis of gene ontology categories for the 232 most radically altered genes, we found that the significant categories related to hepatic function. Furthermore, through the use of small interfering RNA technology *in vitro*, hepatocyte nuclear factor 3β/FoxA2 was identified as having an essential role in hepatic differentiation. These results demonstrate that ES cell–derived hepatocytes recapitulate the gene expression profile of adult mouse liver to a significant degree and indicate that our direct induction system progresses via endoderm differentiation. In conclusion, our system closely mimics *in vivo* hepatic differentiation at the transcriptional level and could, therefore, be useful for studying the molecular basis of hepatocyte differentiation *per se*. (HEPATOLOGY 2005;42: 558-567.)

Embryonic stem (ES) cells have the ability to differentiate into a variety of cell lineages.[1,2] ES cells can be propagated indefinitely in an undifferentiated state but, when provided with the appropriate signals, have the capacity to differentiate—presumably via the formation of precursor cells—into almost any mature cell phenotype. The recapitulation of developmentally regulated gene expression patterns enables the analysis of developmental processes on a cellular level *in vitro*. Therefore, ES cells have been used as a complementary experimental model to analyze early differentiation events *in vivo*. These regulatory genes are often transcriptional factors that activate or repress patterns of gene expression that create the phenotypic change seen during stem cell differentiation.[3,4]

At the molecular level, the induction of liver development and its progress is characterized by the expression of transcription factors, such as hepatocyte nuclear factors (HNFs), CCAAT/enhancer-binding proteins, and GATA-binding proteins. These so-called "liver-enriched" transcription factors show a specific expression pattern during organogenesis with a distinct narrow time interval of transcription initiation.[5,6] Recently, we established the direct differentiation of functional hepatocytes from an adherent monoculture condition of ES cells without forming embryoid bodies and clearly identified the growth factors that direct hepatic fate specification (the hepatic induction factor cocktail [HIFC] differentiation system)[7] based on the *in vivo* induction system.[8] These cells expressed several differentiation markers of mature hepatocytes and rescued experimental liver injury when they were transplanted into animals. Our next goal was to

Abbreviations: ES, embryonic stem; HNF, hepatocyte nuclear factor; HIFC, hepatic induction factor cocktail; siRNA, small interfering RNA; GFP, green fluorescent protein; GO, gene ontology; PCR, polymerase chain reaction; RT-PCR, reverse-transcriptase polymerase chain reaction; ALB, albumin; AFP, alpha-fetoprotein.

From the [1]Section for Studies on Metastasis, National Cancer Center Research Institute, Tokyo, Japan; the [2]Graduate School of Science and Engineering, Waseda University, Tokyo, Japan; the [3]Department of Biochemistry and Molecular Biology, Graduate School of Medicine, The University of Tokyo, Tokyo, Japan; and [4]DNA Chip Research Inc., Yokohama, Japan.

Received January 27, 2005; accepted June 11, 2005.

Supported in part by a Grant-in-Aid for the Third-Term Comprehensive 10-Year Strategy for Cancer Control; Health Science Research Grants for Research on the Human Genome and Gene Therapy from the Ministry of Health, Labor, and Welfare of Japan; and the Program for Promotion of Fundamental Studies in Health Sciences of the Organization for Pharmaceutical Safety and Research of Japan.

Address reprint requests to: Takahiro Ochiya, Ph.D., Head of Section for Studies on Metastasis, National Cancer Center Research Institute, 1-1, Tsukiji 5-chome, Chuo-ku, Tokyo 104-0045, Japan. E-mail: tochiya@ncc.go.jp; fax: (81) 3-3541-2685.

Published online in Wiley InterScience (www.interscience.wiley.com).

DOI 10.1002/hep.20825

Potential conflict of interest: Nothing to report.